

# EGCG/gelatin-doxorubicin gold nanoparticles enhance therapeutic efficacy of doxorubicin for prostate cancer treatment

**Aim:** Development of epigallocatechin gallate (EGCG) and gelatin-doxorubicin conjugate (GLT-DOX)-coated gold nanoparticles (DOX-GLT/EGCG AuNPs) for fluorescence imaging and inhibition of prostate cancer cell growth. **Materials & methods:** AuNPs alternatively coated with EGCG and DOX-GLT conjugates were prepared by a layer-by-layer assembly method. The physicochemical properties of the AuNPs and the effect of Laminin 67R receptor-mediated endocytosis on the anticancer efficacy of the AuNPs were examined. **Results:** The AuNPs significantly inhibit the proliferation of PC-3 cancer cell and the enzyme-responsive intracellular release of DOX could be tracked by monitoring the recovery of the fluorescence signal of DOX. **Conclusion:** Laminin 67R receptor-mediated delivery of DOX using the AuNPs enhanced cellular uptake of DOX and improved apoptosis of PC-3 cells.

**First draft submitted:** 15 June 2015; **Article accepted for publication:** 30 September 2015;  
**Published online:** 11 December 2015

**Keywords:** cellular uptake • doxorubicin • drug release • EGCG • gelatin • gold nanoparticles • Lam 67R • MMP-2 • prostate cancer

There are some disadvantages associated with the treatment of malignant tumors by clinically used anticancer drugs, such as unfavorable pharmacokinetics, serious side effects, drug resistance and poor intracellular uptake, that finally weakened their chemotherapeutic effects in clinical circumstances. To overcome the obstacles, systemic anticancer delivery using nanoscale drug carriers (e.g., drug-polymer conjugates, liposomes, dendrimers and organic/inorganic nanoparticles) have been developed, making a significant impact in cancer therapies [1–4]. Nanocarriers enable passive targeting through the enhanced permeability and retention effect. Moreover, active targeting can be achieved by conjugating nanocarriers with ligands that bind to overexpressed antigens or receptors on the surface of cancer cells, thus facilitating the selective accumulation of anticancer drugs to the intended tissues with no apparent adverse reactions in tumor therapy.

Within the last decade, gold nanoparticles (AuNPs) have attracted much attention in the field of biomedical imaging and clinical diagnostics [5]. The organ distribution of AuNPs is dependent on their size. AuNPs with particle size >10 nm were most often accumulated in blood, liver and spleen [6]. Analysis of AuNP cell/interaction using the Hydra model showed that AuNPs were rapidly internalized by Hydra and then recruited into vacuoles/endosome. The internalized AuNPs were almost complete clearance from the living organism after 48 h [7]. Moreover, AuNPs can be readily functionalized with a variety of molecules and ligand to achieve efficacy and limit off-target toxicity [8]. The drug carrying AuNPs were allowed to navigate tissue for detecting diseases in a noninvasive and real-time monitoring manner, and releasing drugs into their targets for therapeutic purposes [9]. Modification of AuNPs with tumor-specific, stimuli-responsive mol-

Li-Chu Tsai<sup>1</sup>, Hao-Ying Hsieh<sup>1,2</sup>, Kun-Ying Lu<sup>3</sup>, Sin-Yu Wang<sup>3</sup> & Fwu-Long Mi<sup>\*,3,4,5</sup>

<sup>1</sup>Institute of Organic & Polymeric Materials, National Taipei University of Technology, Taipei 10608, Taiwan

<sup>2</sup>Institute of Biomedical Engineering, National Taiwan University, Taipei 10002, Taiwan

<sup>3</sup>Graduate Institute of Medical Sciences, College of Medicine, Taipei Medical University, Taipei 11031, Taiwan

<sup>4</sup>Department of Biochemistry & Molecular Cell Biology, School of Medicine, College of Medicine, Taipei Medical University, Taipei City 11031, Taiwan

<sup>5</sup>Graduate Institute of Nanomedicine & Medical Engineering, College of Biomedical Engineering, Taipei Medical University, Taipei 11031, Taiwan

\*Author for correspondence:

Fax: +886 227 356 689

[flmi530326@tmu.edu.tw](mailto:flmi530326@tmu.edu.tw)

ecules can be an effective strategy to make AuNPs a controllable release system for the specific targeting diagnosis and therapeutics [10].

Doxorubicin (DOX) is a drug used in cancer chemotherapy for the treatment of a wide range of carcinoma and soft tissue sarcomas. However, DOX-associated cardiotoxicity caused by poor targeting of DOX to tumor cells and the multidrug resistance effect has decreased in availability of DOX for cancer therapy application. Doxil® is the first US FDA-approved cancer nanomedicine which can be passively targeted to tumors and has decreased cardiotoxicity compared with free doxorubicin [11]. Recently, the methods of encapsulation of DOX in micelles or conjugation of DOX to nanoparticles have been developed to overcome these disadvantages [12–14]. Consequently, the therapeutic efficacy was enhanced due to dramatic alteration in the chemotherapeutic pharmacokinetics and biodistribution of DOX [15,16]. Although there have been numbers of work on the development of nanocarriers for DOX delivery [11–14,17], the issues of prostate cancer targeted therapy in stimuli-responsive fluorescence imaging and drug release are still not found.

Epigallocatechin gallate (EGCG), the major component in tea polyphenols, has been known to have protective effects against the development and progression of prostate cancer [18,19]. EGCG can induce apoptotic cell death, influence cell signals and gene expression, and modulate the activities of specific enzymes, consequently inhibiting the growth of prostate cancer [20]. Previous studies reported that EGCG can effectively reduce tetrachloroaurate (III) ions to AuNPs and also serve as an excellent stabilizer to prevent the created AuNPs from agglomeration by the formation of EGCG-shielded AuNPs [21,22]. Furthermore, EGCG can specifically bind to the laminin receptor overexpressed in some cancer cells [23,24]. Intratumoral injection of EGCG-functionalized <sup>198</sup>Au NPs in prostate tumor-bearing mice showed high retention of the radioactive AuNPs in tumors and effective reduction of tumor volumes [21]. Another study reported that micellar nanocomplexes comprising EGCG and Herceptin® showed superior tumor selectivity and growth reduction than free Herceptin [25]. It is therefore reasonable to hypothesize that EGCG effectively improves the internalization of nanoparticles in various types of cancer cells including prostate cancer.

It is well known that matrix metalloproteinases (MMPs) that are highly expressed in the tumor micro-environment (intracellular and extracellular) play an important role in invasion and metastasis of cancer by cleaving collagen and its denatured form gelatin. Wong *et al.* developed an engineered nanoparticle with a core composed of gelatin and a surface covered

with quantum dots. MMP-2 triggered the shrinkage of the nanoparticles, facilitating deep penetration of the nanoparticles into tumor tissues [26]. Another study reported the preparation of supramolecular gelatin nanoparticles as MMP responsive cancer cell imaging probes [27]. Our study aimed to develop 67-kDa laminin receptor (67LR)-targetable and MMP-responsive nanoparticles for targeted DOX delivery. DOX was conjugated with gelatin (GLT) and EGCG-functionalized AuNPs (EGCG AuNPs) were prepared by reduction of tetrachloroaurate (III) ions in EGCG aqueous solution. Based on the knowledge of high-affinity binding of EGCG to GLT [28], DOX-GLT can be effectively incorporated into the EGCG AuNPs. In this study, DOX-GLT was coated on the surface of EGCG AuNPs by a layer-by-layer assembly method (Figure 1). *In vitro* release of DOX from DOX-GLT/EGCG AuNPs was determined in the MMP-2-containing medium. We show effective accumulation of the DOX-GLT/EGCG AuNPs in PC-3 cells and significant inhibition of the cancer cells proliferation because the nanoparticles were increasingly uptaken by the cells via receptor-mediated endocytosis. We also find that the cellular uptake and inhibition of PC-3 cells proliferation became less evident after block of 67LR.

## Materials & methods

### Materials

EGCG (98%) was purchased from Zhejiang Yixin Pharmaceutical Co., Ltd. (Zhejiang, China). Type B gelatin (from bovine skin, gel strength ~225 g Bloom) and DOX were purchased from Sigma-Aldrich Company Ltd. (MO, USA). Methanol (MeOH) (HPLC grade) and acetonitrile (ACN) (HPLC grade) were obtained from Mallinckrodt Baker (NJ, USA).

### Preparation & characterization of epigallocatechin gallate-gold nanoparticles

The EGCG solution (0.2, 0.15, 0.1 or 0.05 wt%) was prepared by vigorous stirring of EGCG in deionized (DI) water and stirred continuously at 25°C for 15 min. Subsequently, 1 ml of 4.0, 2.0, 1.0, 0.75, 0.5 and 0.25 mM HAuCl<sub>4</sub> solution was added dropwise into 1 ml of previously prepared EGCG solution at 25°C with magnetic stirring. The color of the solution gradually changed from pale yellow to purple over a period of 10 min. After the color change, stirring is continued for 15 min to ensure a complete reaction. The samples were respectively noted as EGCG<sub>0.20</sub>-Au<sub>4.0</sub> NPs, EGCG<sub>0.20</sub>-Au<sub>2.0</sub> NPs, EGCG<sub>0.05</sub>-Au<sub>0.25</sub> NPs, etc. Absorption spectra of the samples were investigated by utilizing a UV-Vis spectrophotometer (Hitachi, Tokyo, Japan). The mean particle sizes and zeta potential values of EGCG-AuNPs were determined by

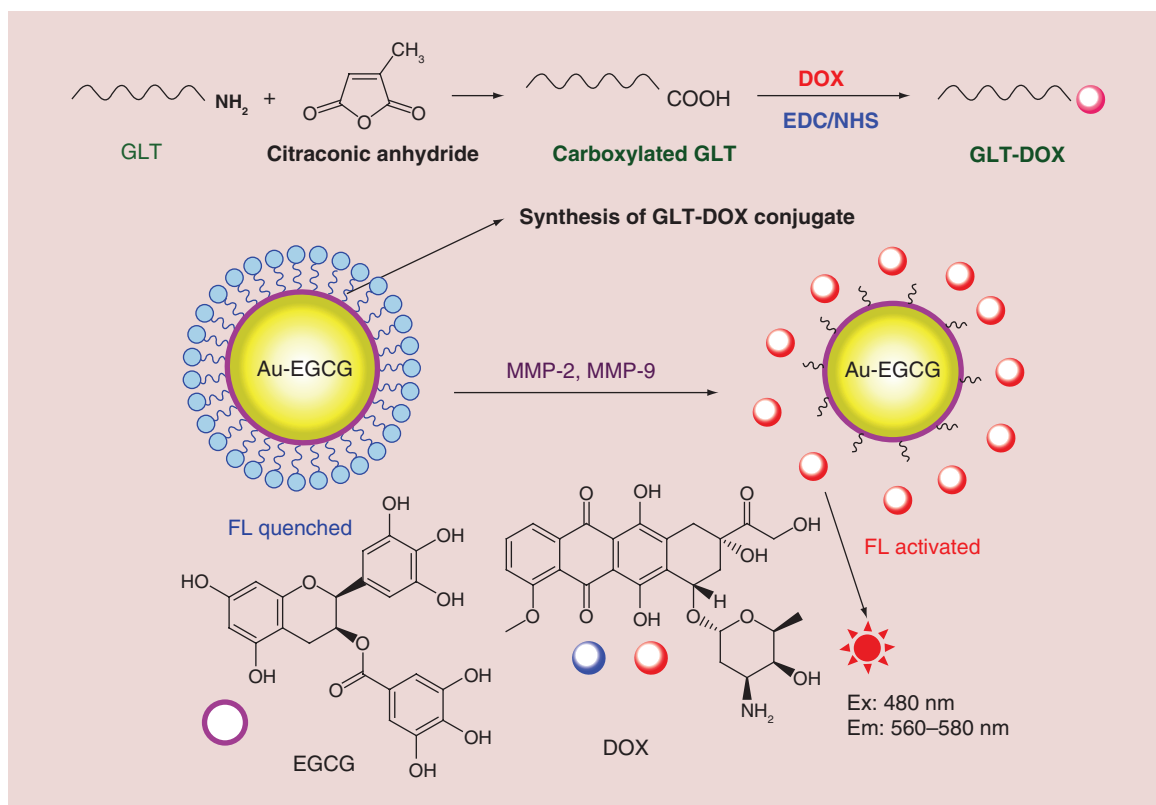


**Figure 1. Schematic diagram showing the synthesis and optical properties of layer-by-layer assembled GLT-DOX/EGCG-AuNPs.**

AuNP: Gold nanoparticle; DOX: Doxorubicin; EGCG: Epigallocatechin gallate; FL: Fluorescence; GLT: Gelatin.

a dynamic light-scattering technique using a Malvern 3000HS Zetasizer. The nanoparticle suspensions were dropped on to a copper grid and allowed to air dry after deposition of the nanoparticles. The morphology and structure of EGCG-AuNPs were examined by transmission electron microscopy (TEM) coupled with energy-dispersive x-ray spectroscopy. Raman spectra of EGCG-AuNPs were recorded on a Renishaw inVia Raman microscope over the range of 300–3000  $\text{cm}^{-1}$ .

### Characterization of interactions between epigallocatechin gallate & gelatin

Interactions of EGCG and GLT were examined by a circular dichroism (CD) and isothermal titration calorimetry (ITC) method. CD spectra were scanned at a speed of 25  $\text{nm min}^{-1}$  with a slit width of 1 nm using a Jasco 715 circular dichroism spectropolarimeter. The spectra were recorded in the far UV region (190–280 nm) under  $\text{N}_2$  atmosphere to estimate the conformational change of GLT brought about by EGCG solution. An aqueous solution of GLT (0.03 wt%, 1 ml) was added with EGCG (0.2 wt%) solution at different volumes (20, 40, 60 and 80  $\mu\text{l}$ ). After subtracting the reference spectrum (solvent peak), the data were normally plotted as mean-residue-weight ellipticity (deg.

$\text{cm}^2 \text{dmol}^{-1}$ ) versus wavelength in nanometer. Changes in the conformation of GLT on addition of various amounts of EGCG were recorded.

The thermodynamics of the binding of GLT to EGCG was assessed using a Nano ITC Isothermal Titration Calorimetry (TA Instruments, DE, USA). The reference cell was filled with deionized water while the sample cell was filled with GLT solution (0.2 mM, 1100  $\mu\text{l}$ ). The injection syringe was filled with 8 mM EGCG solution and was titrated into the sample cell as a sequence of 20 injections of 5  $\mu\text{l}$  aliquots under 250 rpm stirring at 298 K. Data acquisition was performed with NanoAnalyze software (TA Instruments) and was shown as a plot of observed enthalpy change per mole of injectant ( $\Delta H_{\text{obs}}$ ,  $\text{kJ mol}^{-1}$ ) against molar ratio. Equilibrium binding constants, heats of binding and stoichiometries were determined by nonlinear least-squares fitting for ITC data analysis.

### Synthesis & characterization of doxorubicin-gelatin conjugates

An amount of gelatin was dissolved in water to obtain a stock gelatin solution (10 mg/ml). The stock solution was diluted to 4 mg/ml and subsequently reacted with citraconic anhydride (22.1 mM) at a citraconic

anhydride-to-GLT weight ratio of 0.62. After 2 h of reaction at room temperature, the final product (a carboxylated GLT) was dialyzed against water for 72 h using a dialysis membrane (molecular weight cut-off 10,000, Spectra/Por®) and lyophilized. The lyophilized product (250 mg dissolved in 50 ml DI water) was allowed to react with 50 mg of EDC (5.23 mM) to activate the carboxyl groups. After 30 min, 96 mg of DOX (3.31 mM) was added to the carboxylated GLT (5 mg/ml)/EDC (5.23 mM) mixture and the reaction was maintained at pH 5.0 for 24 h to obtain the DOX-GLT conjugate. The Fourier transform infrared (FTIR) spectra of the lyophilized compounds were recorded on a Perkin-Elmer Spectrum RX1 spectrometer in the region 400–4000 cm<sup>-1</sup> with the samples taken as KBr pellets. Amount of covalently bound DOX in the DOX-GLT conjugate was calculated from the absorbance measured by a UV-Vis spectrophotometer (Hitachi 250 UV-Vis, Tokyo, Japan) at 485 nm.

#### Synthesis of layer-by-layer assembled doxorubicin-gelatin/epigallocatechin gallate-gold nanoparticles

The previously prepared EGCE-AuNPs (2 ml) were added to 2.0 mg/ml DOX-GLT conjugate aqueous solution (2 ml) under stirring. After 10 min, the DOX-GLT-coated EGCE-AuNPs were centrifuged (10000 × g rpm) and washed to eliminate the excess of DOX-GLT. The centrifuged AuNPs (2 mg) were mixed with 0.2 wt% EGCG solution (1 ml) and the reaction was allowed to continue for 10 min. The AuNPs were alternatively coated with EGCE and DOX-GLT to obtain a layer-by-layer assembled DOX-GLT/EGCG-AuNPs. The DOX and EGCG equivalents in the AuNPs were determined by a UV-Vis spectrophotometer (Hitachi 250 UV-Vis, Tokyo, Japan) at 485 and 285 nm, respectively.

#### Nanoparticle surface-energy transfer measurements

The EGCE-AuNPs and DOX-GLT conjugates were synthesized according to the above-mentioned process. Fluorescence spectra of the DOX-GLT conjugate was determined by a Hitachi fluorescence spectrophotometer (F-2500, Japan) using an excitation wavelength of 485 nm. The nanoparticle surface energy transfer (NSET) effect was investigated by titrating DOX-GLT conjugate with EGCG-AuNPs and the fluorescence spectra were recorded. An amount of EGCG-AuNPs (0–500 μl) was added to 1 ml of DOX-GLT conjugate aqueous solution (2.0 mg/ml) to form DOX-GLT/EGCG-AuNPs nanocomplex and the emission spectrum of the complex was recorded to determine the ratio of the complex-to-original emission intensity (IC/IO). The dissociation of DOX from the nanocomplex

was examined by keeping the nanocomplexes in the medium containing MMP-2 (50–1000 ng/ml), and the recovery of fluorescence was recorded.

#### Release of doxorubicin from gold nanoparticles

The pH-dependent DOX release measurements were carried out by suspending the DOX-GLT/EGCG-AuNPs nanocomplex (100 mg) in 10 ml of PBS with or without MMP-2 (1.0 μg/ml). At predetermined time intervals, the nanoparticle dispersion was centrifuged, the supernatants were collected and replaced with the same volume of fresh medium. The amount of DOX released was calculated from the absorbance measured by a UV-Vis spectrophotometer (Hitachi 250 UV-Vis, Tokyo, Japan) at 485 nm.

#### Intracellular uptake of doxorubicin

Metastasized human prostate cancer cells (PC-3) were grown and maintained in RPMI 1640 culture medium. The medium contained 10% fetal bovine serum and the temperature of the CO<sub>2</sub> (5%) incubator was kept at 37°C. The PC-3 cells (2.5 × 10<sup>5</sup> cells/ml) were plated in 24-well cell culture plates and allowed to grow overnight. The cells were sequentially treated with Lam 67R-specific MLuC5 antibody (NeoMarkers, CA, USA) and secondary antibody (Alexa 594, DAKO, CA, USA). Subsequent to blocking the Lam 67R receptors, the PC-3 cells were treated with DOX-GLT/EGCG-Au NPs (2 mg/ml of DOX equivalent) for 90 min. For negative control experiments, the cells were incubated with a nonimmune serum instead of primary antibody. The coverslips with growing cells were briefly washed with PBS, fixed in freshly made 4% paraformaldehyde. The cells were counterstained with the nuclear marker DAPI. The coverslips was examined using a laser scanning confocal microscope (TCS-SP5, Leica, Germany).

PC-3 cells incubated with AuNPs were harvested after trypsin treatment, and the cells were fixed in PBS containing 2.5% glutaraldehyde for 12 h, dehydrated in ethanol before embedding into Epon Araldite resin, and then stained with 4% uranyl acetate. An ultrathin section was cut on an MT-X Ultra microtome using a 45 diatom diamond knife, and then placed on the grids for observation under the transmission electron microscope (H-7650B).

#### Measurements of doxorubicin retention by flow cytometry

DOX-GLT/EGCG-AuNPs were obtained from the above-mentioned process. DOX-GLT/AuNPs were prepared according to the procedure of Neupane *et al.* [29]. DOX-GLT-capped AuNPs were prepared by reduction of HAuCl<sub>4</sub> solution (1 mM) with

sodium citrate (38.8 mM) using DOX-GLT (2 mg/ml) as a stabilizing reagent. PC-3 cells were respectively incubated with DOX-GLT/EGCG-AuNPs or DOX-GLT/AuNPs for 2 h. The cells were washed twice with PBS after harvesting the cells by trypsin/EDTA treatment. Intracellular accumulation and retention of DOX was measured by using a FACSCanto flow cytometer (FACSCanto, Becton Dickinson, CA, USA).

### **In vitro anticancer assay**

PC-3 cells were seeded and incubated according to the above-mentioned procedure. After 24 h of incubation, EGCG-AuNPs, DOX-GLT/AuNPs and DOX-GLT/EGCG-AuNPs were added to the culture medium at different DOX and EGCG equivalents. The cells were further incubated for 48 h, and then MTT assay was used to quantify cell viability by determining the absorbance of dissolved formazan crystal using a Perkin Elmer EnSpire 2300 multimode plate reader at 570 nm. Cytotoxicity was expressed as the relative viability (% control).

### **Statistical analysis**

Statistical analysis was performed using one-way analysis (ANOVA) followed by Tukey's post-test; \* $p < 0.05$ , \*\* $p < 0.01$ . Results are expressed as mean and standard error of mean.

## **Results & discussion**

### **Characterization of epigallocatechin gallate-gold nanoparticles**

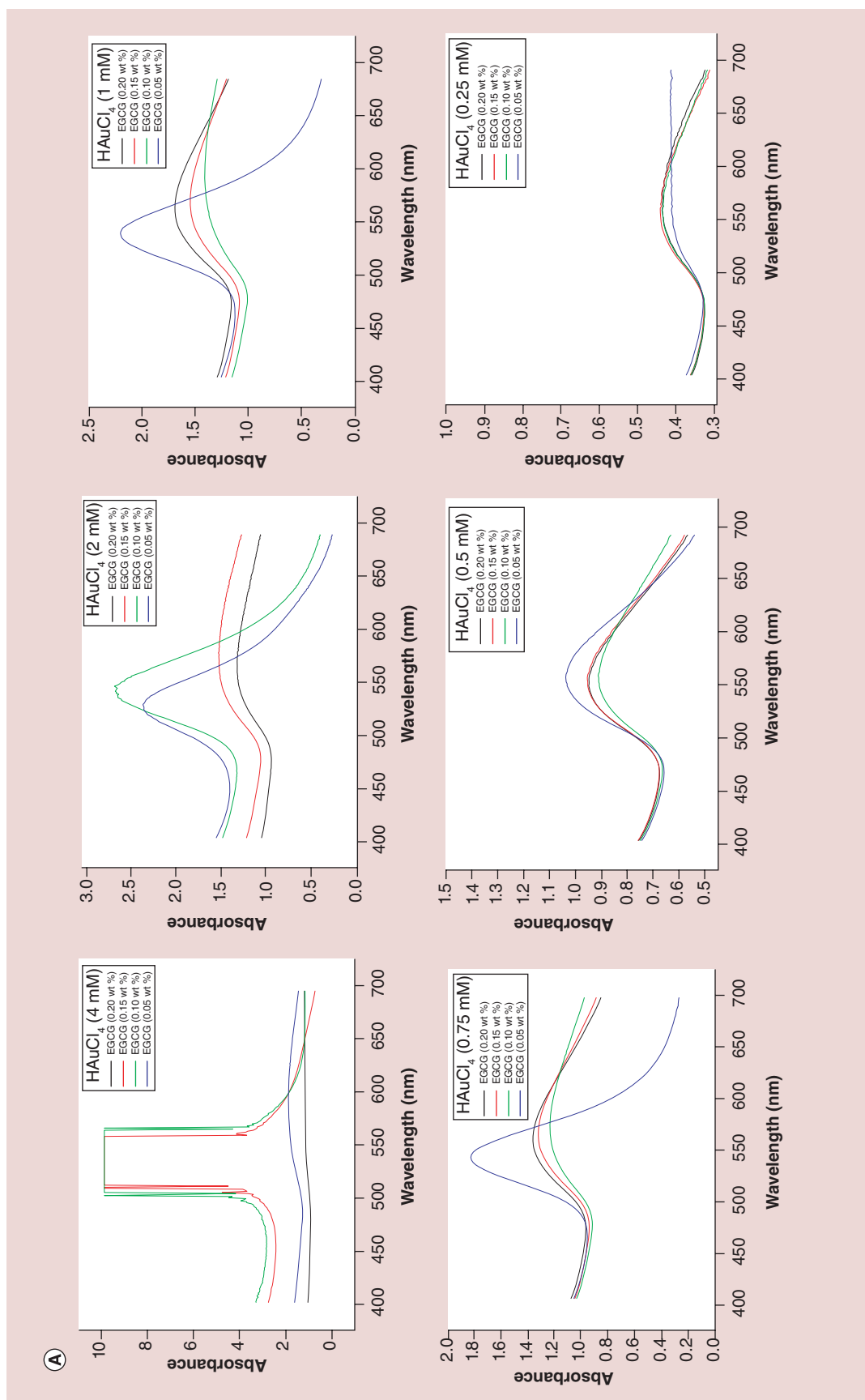
In this work, EGCG was not only used as a reducing agent but also as a stabilizing agent for preparing the EGCG-capped AuNPs (EGCG-AuNPs). The color of the prepared AuNP dispersions changed from red to blue because surface plasmon resonance (SPR) frequency highly depends on the size and shape of the nanoparticles. UV-Vis absorption spectrum of gold nanoparticles dispersed in water generally exhibits the SPR at around 540 nm, which is attributed to the in-plane dipole resonance. Generally, the SPR absorption intensity increased with increasing the concentration of  $\text{HAuCl}_4$ . High concentrations of  $\text{HAuCl}_4$  (2 and 4 mM) facilitated the formation of EGCG-AuNPs with intense SPR absorption peaks (Figure 2A). As the concentration of EGCG increased, the SPR absorption bands of the EGCG-AuNPs were red-shifted, indicating the formation of larger sizes of nanoparticles. The change in SPR absorption band reveals that EGCG plays an important role to disperse and stabilize the AuNPs. EGCG is a polyphenol containing a large number of orthophenolic hydroxyls, which serves as a bidentate ligand that forms complex with  $\text{Au}^{3+}$  ions and could effectively reduce the chelated  $\text{Au}^{3+}$  ions to AuNPs [30].

The EGCG-AuNPs ( $\text{EGCG}_{0.10}\text{-Au}_{4.0}$ ,  $\text{EGCG}_{0.15}\text{-Au}_{4.0}$ ,  $\text{EGCG}_{0.10}\text{-Au}_{2.0}$ , and  $\text{EGCG}_{0.05}\text{-Au}_{2.0}$  NPs) demonstrating stronger SPR absorption in Figure 2A were selected for subsequent measurement of their particle sizes by using dynamic light scattering. Figure 2B shows the particle size distribution of the EGCG-AuNPs. The particle sizes of the EGCG-AuNPs varied in the range from 35 to 85 nm. The high-resolution TEM micrograph of an individual  $\text{EGCG}_{0.10}\text{-Au}_{4.0}$  NPs in Figure 2C clearly shows that the particle sizes of the AuNPs were about 20 nm, which were smaller than those measured by dynamic light scattering. The energy-dispersive X-ray spectroscopy quantitative analysis suggested that the  $\text{EGCG}_{0.10}\text{-Au}_{4.0}$  NPs contained Au (80.07%), C (18.54%) and O (1.37%). This result confirms that EGCG was anchored to the surface of AuNPs for stabilization of the nanoparticles (Figure 2C). Figure 2D shows the Raman spectra of the  $\text{EGCG}_{0.10}\text{-Au}_{4.0}$ ,  $\text{EGCG}_{0.15}\text{-Au}_{4.0}$ ,  $\text{EGCG}_{0.10}\text{-Au}_{2.0}$  and  $\text{EGCG}_{0.05}\text{-Au}_{2.0}$  NPs. As shown in this figure, the intensity of the surface enhanced Raman scattering (SERS) was highest for EGCG0.05-Au2.0 NPs. The SERS intensity of the band in the region from 1500 to 1600  $\text{cm}^{-1}$  was dramatically increased, suggesting that EGCG was effectively bound to the gold surface.

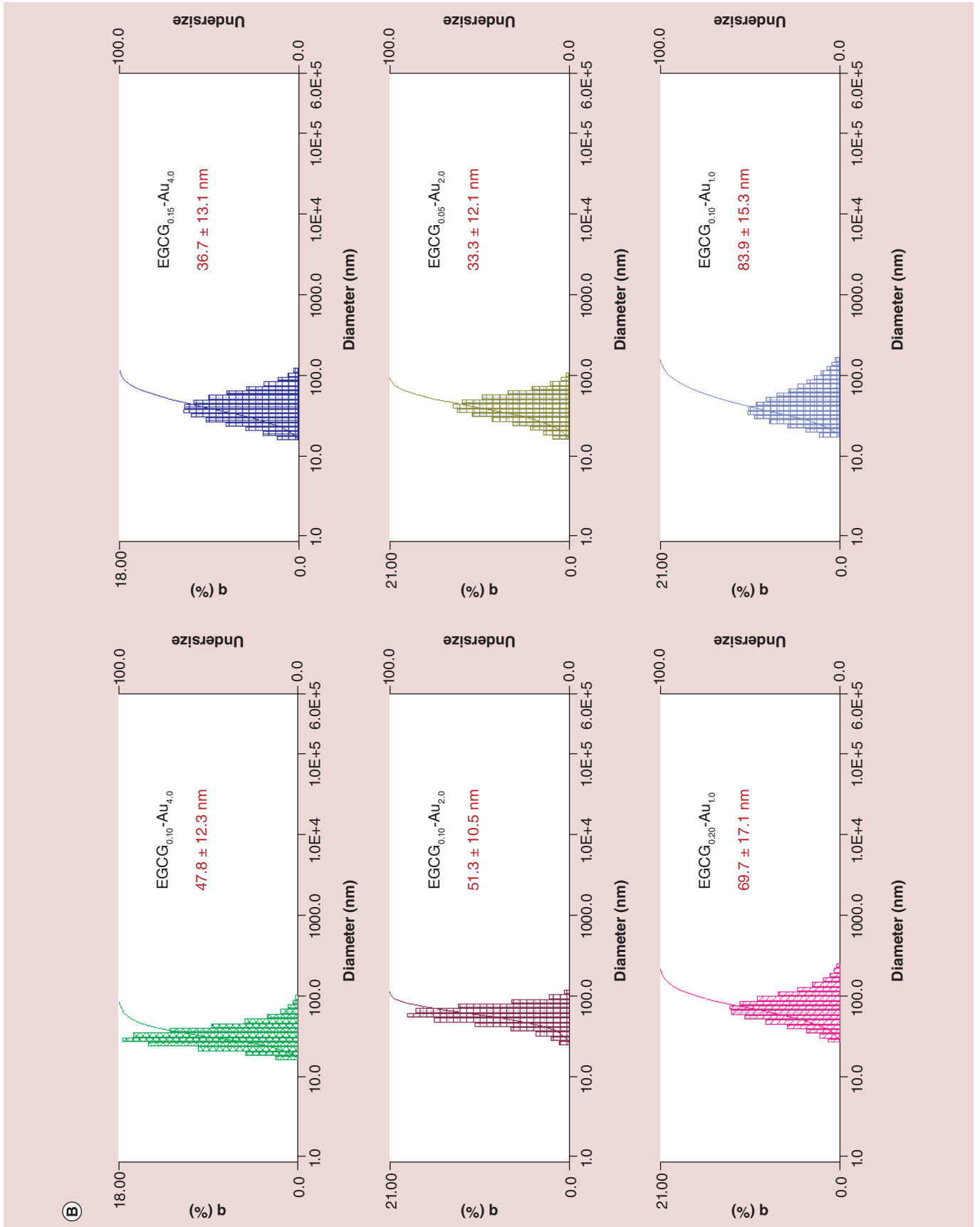
EGCG consisting of abundant orthophenolic hydroxyls is a polyphenolic ligand of Au(III) ions. EGCG-Au(III) complexes are stabilized with the bidentate ligand that forms a five-member ring with Au(III) ions [31]. Subsequent to the chelation reaction, the highly reductive Au(III) ions are readily reduced into Au(0) atoms, accompanied with the polyphenol-quinone oxidation. EGCG-capped NPs are stabilized by the interaction between the surface Au(0) atom of AuNPs and the hydroxyls and quinones in EGCG, resulting in the formation of supramolecularly assembled EGCG-Au(0) complex surface layer providing an efficient steric hindrance to prevent particles aggregation.

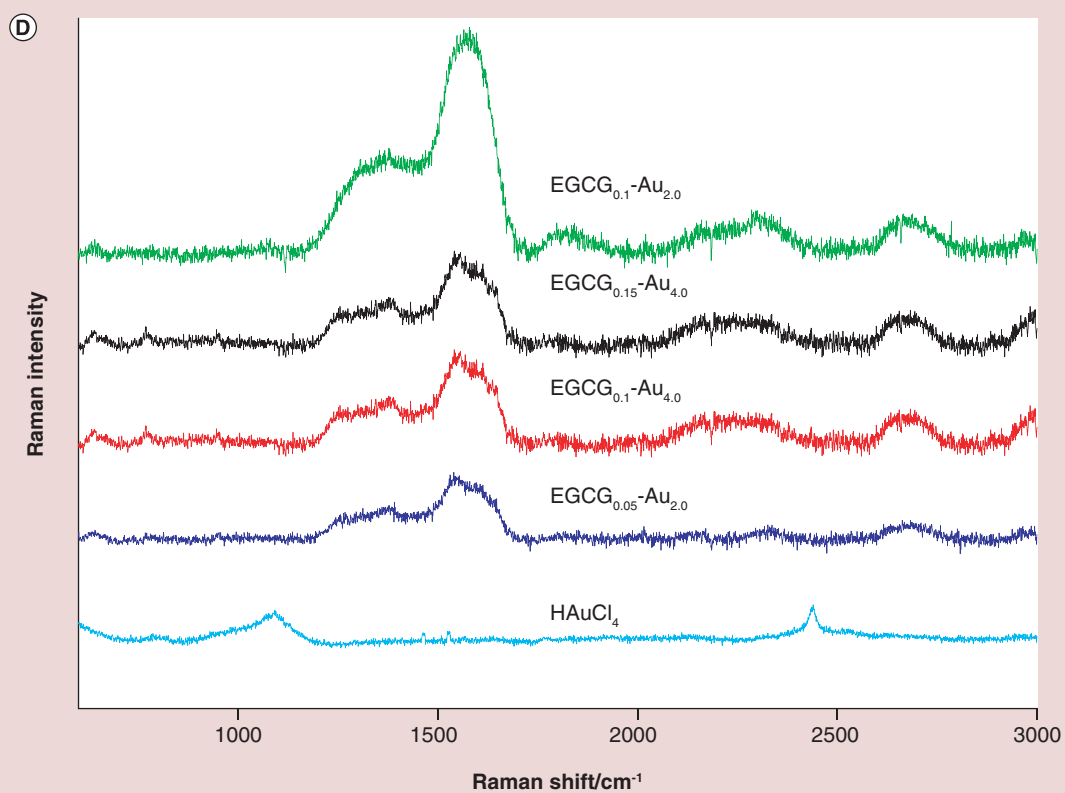
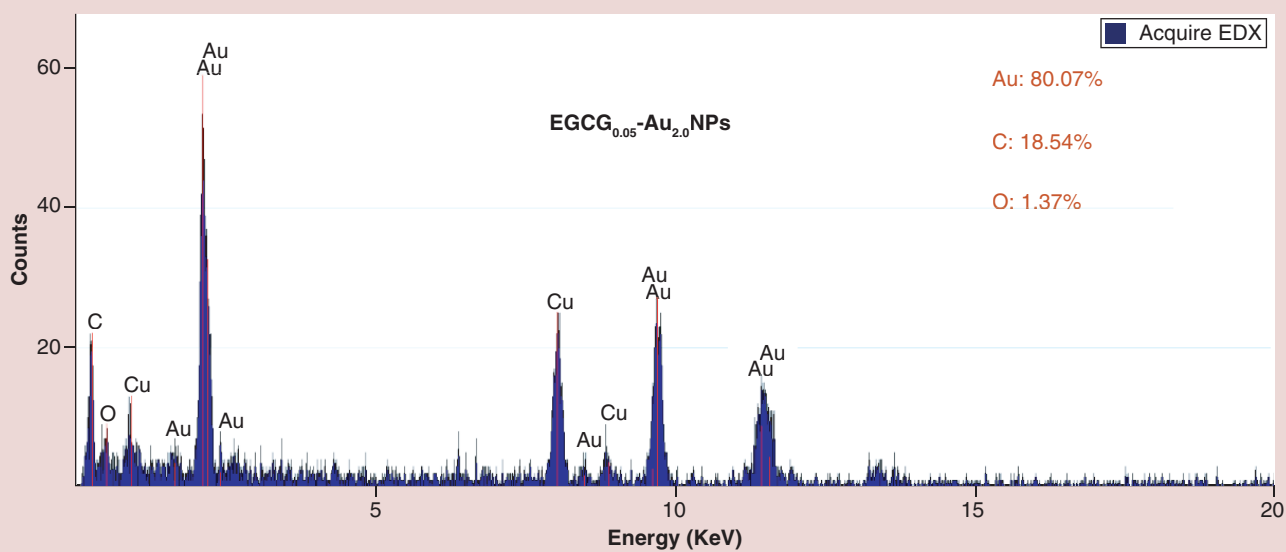
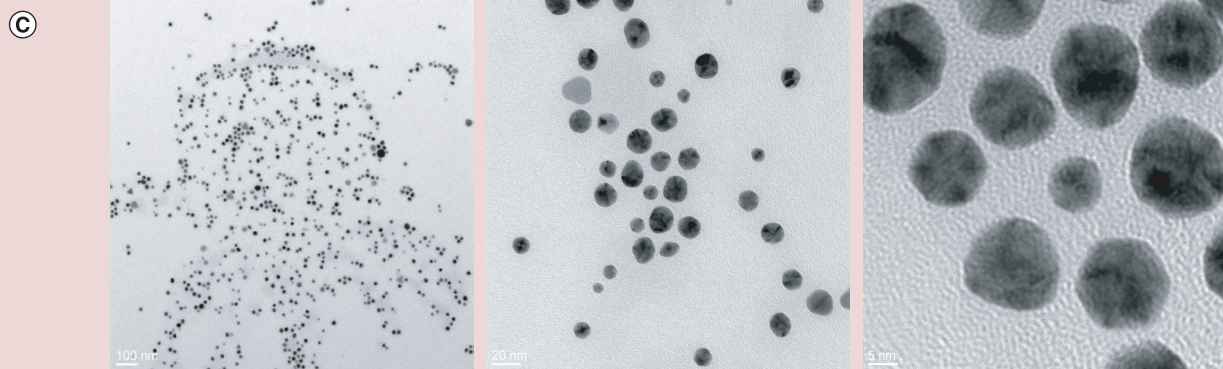
### **Interactions between gelatin & epigallocatechin gallate**

As shown in Figure 3A, GLT and its GLT/EGCG complex can be characterized by CD spectra in the far-ultraviolet wavelength range (190–250 nm) because the spectrum provides secondary structural information of their polypeptide backbone. To gain information on EGCG and GLT interactions, the changes in secondary structure of GLT were examined by CD spectra at various EGCG-to-GLT weight ratios. It has been reported that the coexistence of the bands with negative ellipticity around 198 nm and the band with positive ellipticity at 223 nm is characteristic for triple helical conformation of collagen [32]. The GLT conju-



**Figure 2. Characterization of EGCG-AuNPs prepared at different conditions (please see following two pages for [B-D]).** (A) Absorption spectra. (B) Particle size distribution. (C) Transmission electron microscopy and energy-dispersive x-ray spectroscopy. (D) Raman spectra. AUNP: Gold nanoparticle; EGCG: Epigallocatechin gallate.





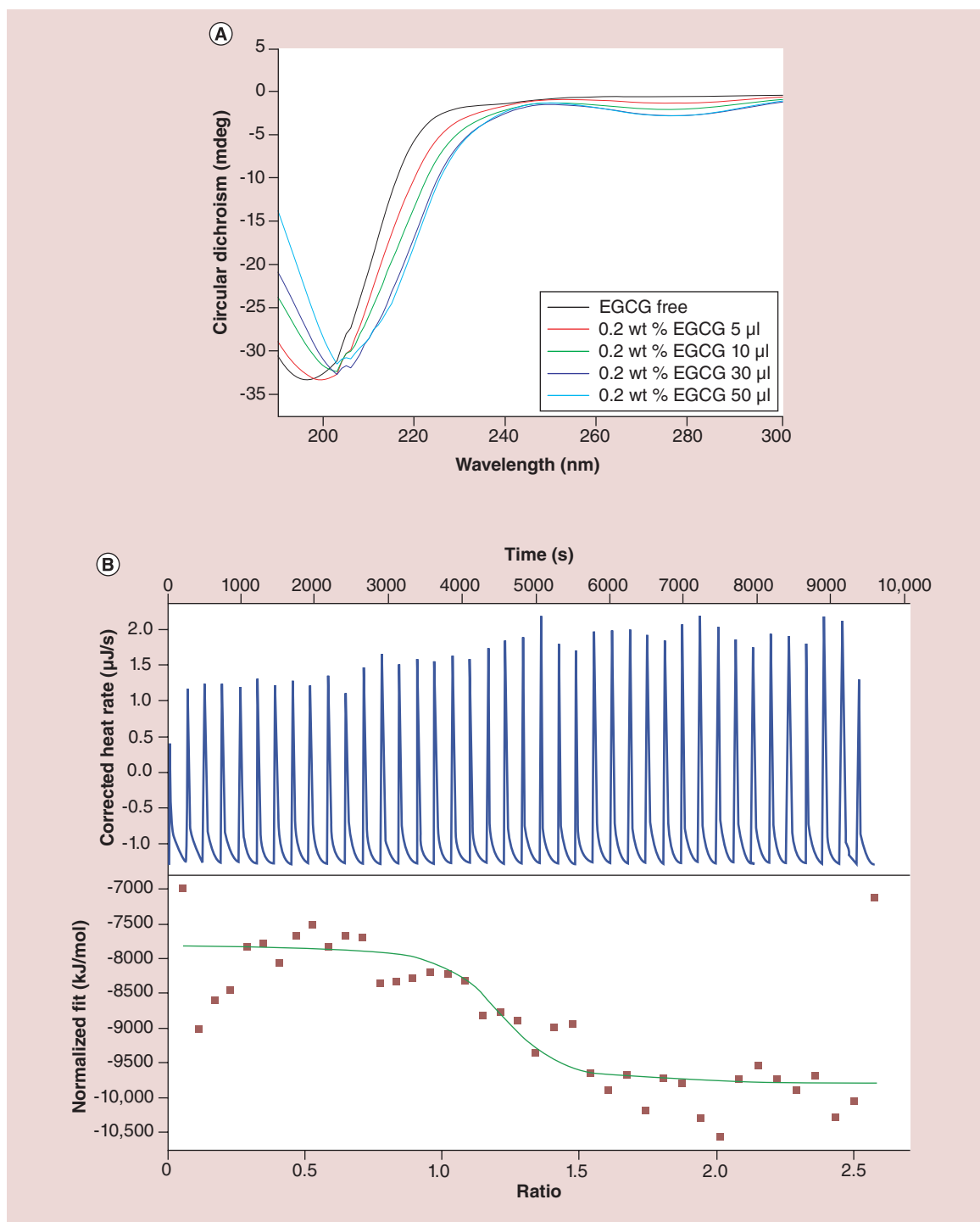


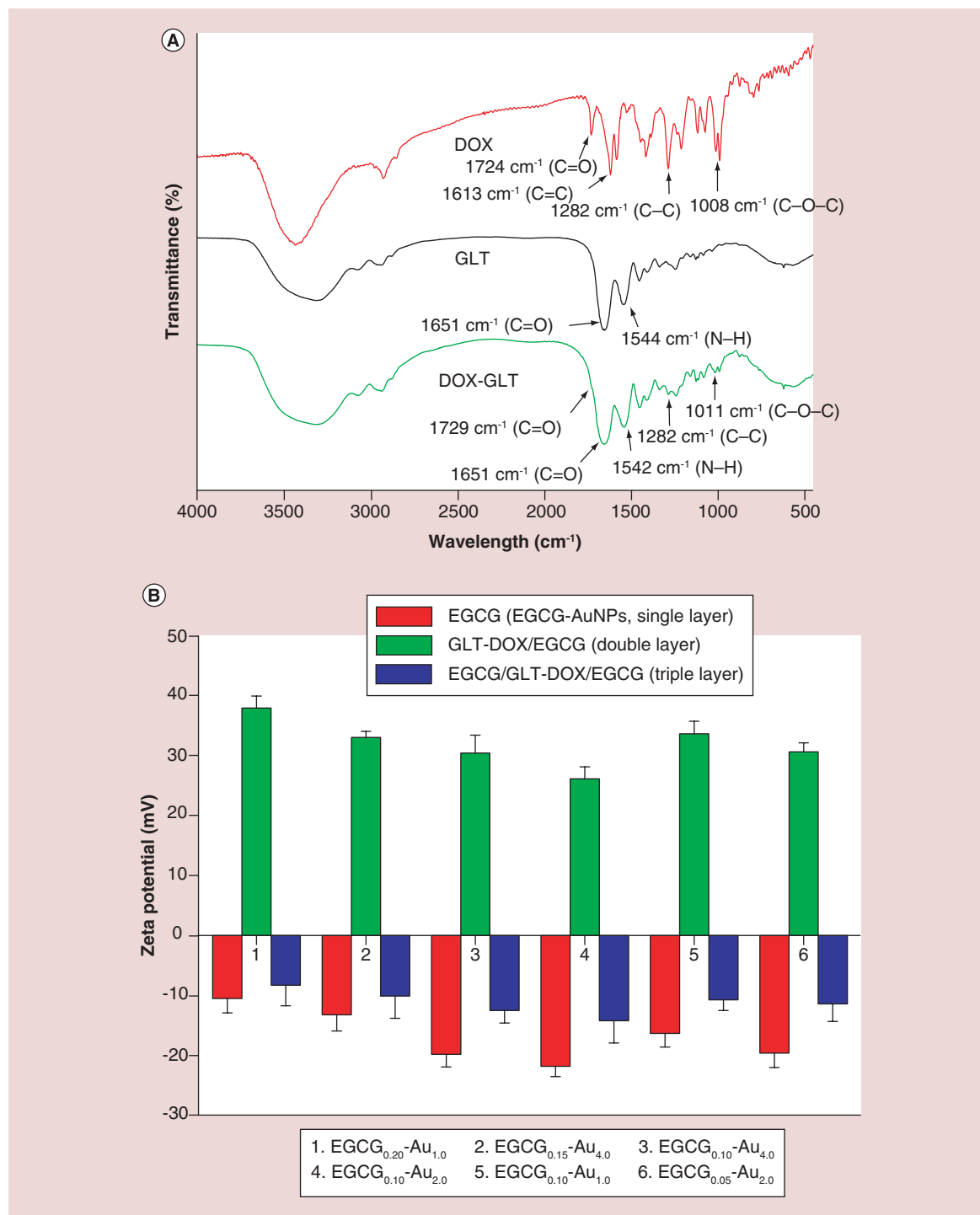
**Figure 3. Circular dichroism spectra and isothermal titration calorimetry analysis.** (A) Circular dichroism spectra of the changes in secondary structure of gelatin (0.03 wt%, 1 ml) upon addition of EGCG (0.2 wt%) solution at different volumes (5, 10, 30 and 50 μl). (B) Isothermal titration calorimetry binding isotherms and heat flow against time for titration of 0.2 mM gelatin with 8 mM EGCG at 298 K. EGCG: Epigallocatechin gallate.

gate demonstrated only a strong peak of negative ellipticity near 195 nm, revealing a pattern characteristic of random-coil conformation of GLT. After adding EGCG to GLT solutions, the peak of negative ellipticity

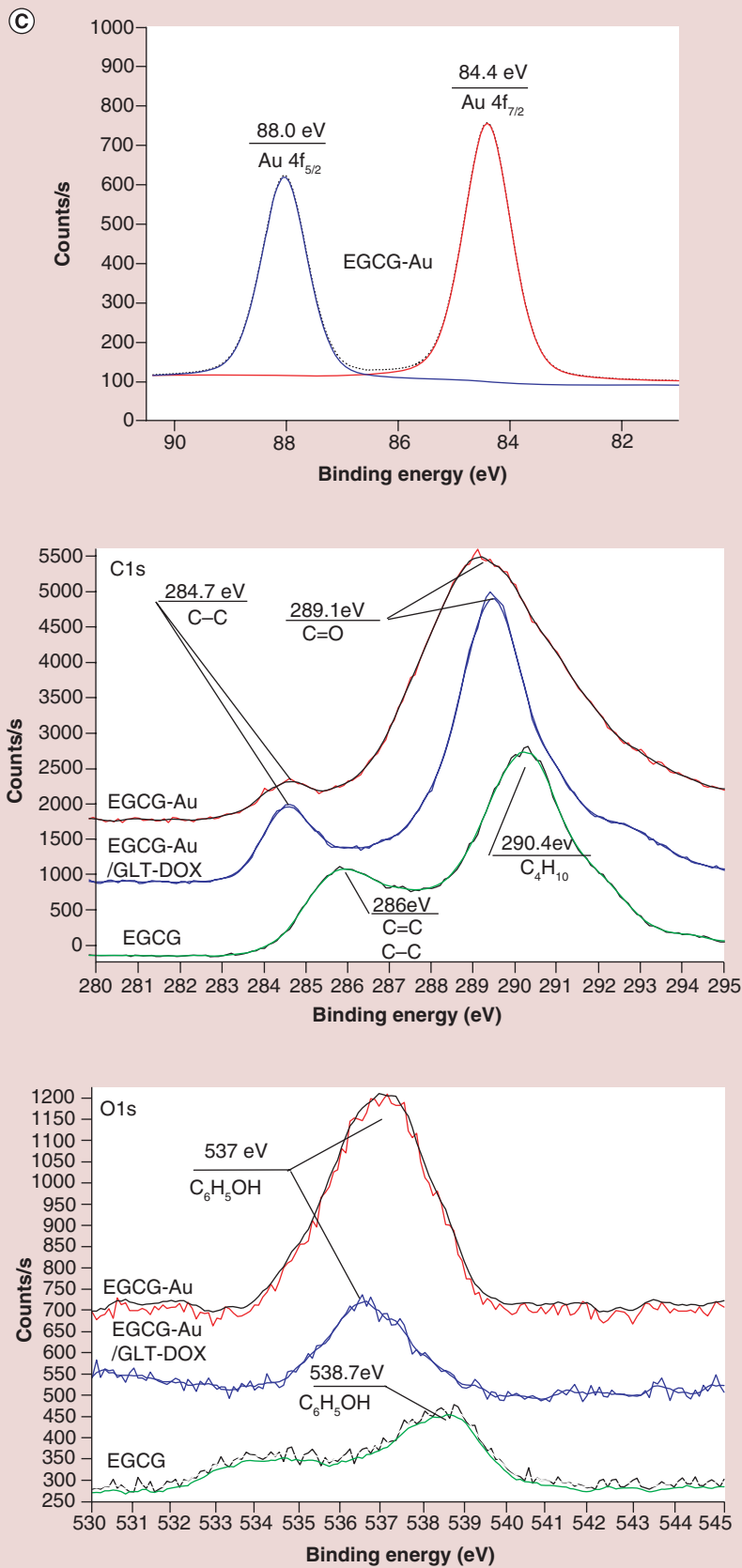
was red shift and the strength decreased with the increase of EGCG content. Furthermore, the peak of negative ellipticity appeared at 280 nm due to the interactions between the polyphenol and the aromatic

residues of GLT. This result suggested that GLT might be reassembled to form the triple helical-like structure by noncovalent interaction with EGCG, due to the protein folding-unfolding effect.

ITC binding isotherms were shown as a plot of heat flow against EGCG-to-GLT molar ratio for the interaction of EGCG with GLT (Figure 3B). An exothermic interaction suggested a strong binding of EGCG with



**Figure 4. FTIR and XPS spectra and zeta potential (for [A & B], please see above; for [C], please see facing page).** (A) FTIR spectra of GLT, DOX and GLT-DOX conjugates, (B) XPS spectra of GLT-DOX/EGCG-AuNPs, (C) zeta potential of various AuNPs prepared by layer-by-layer assembly of EGCG and GLT-DOX multilayers. AuNP: Gold nanoparticle; DOX: Doxorubicin; EGCG: Epigallocatechin gallate; GLT: Gelatin.



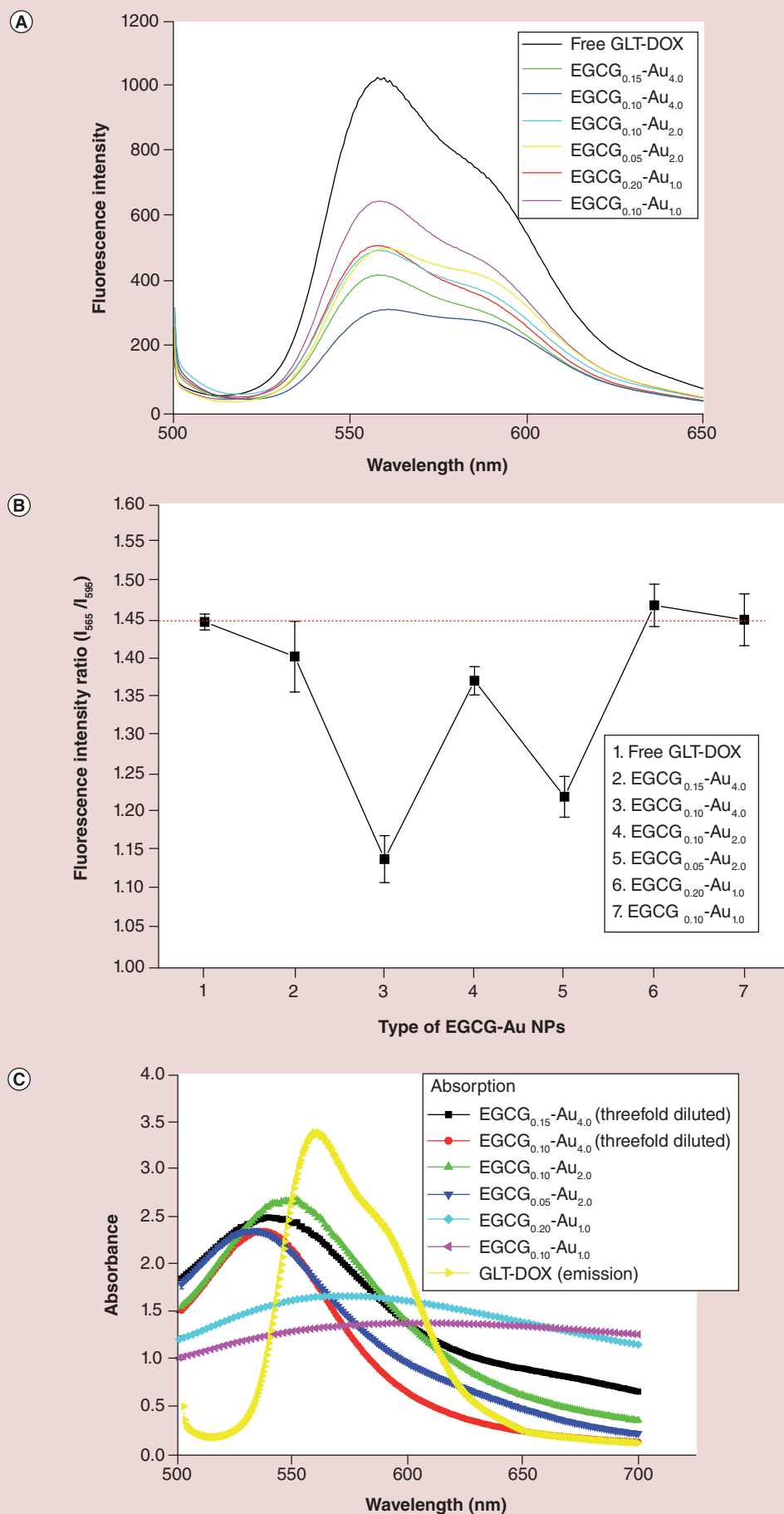
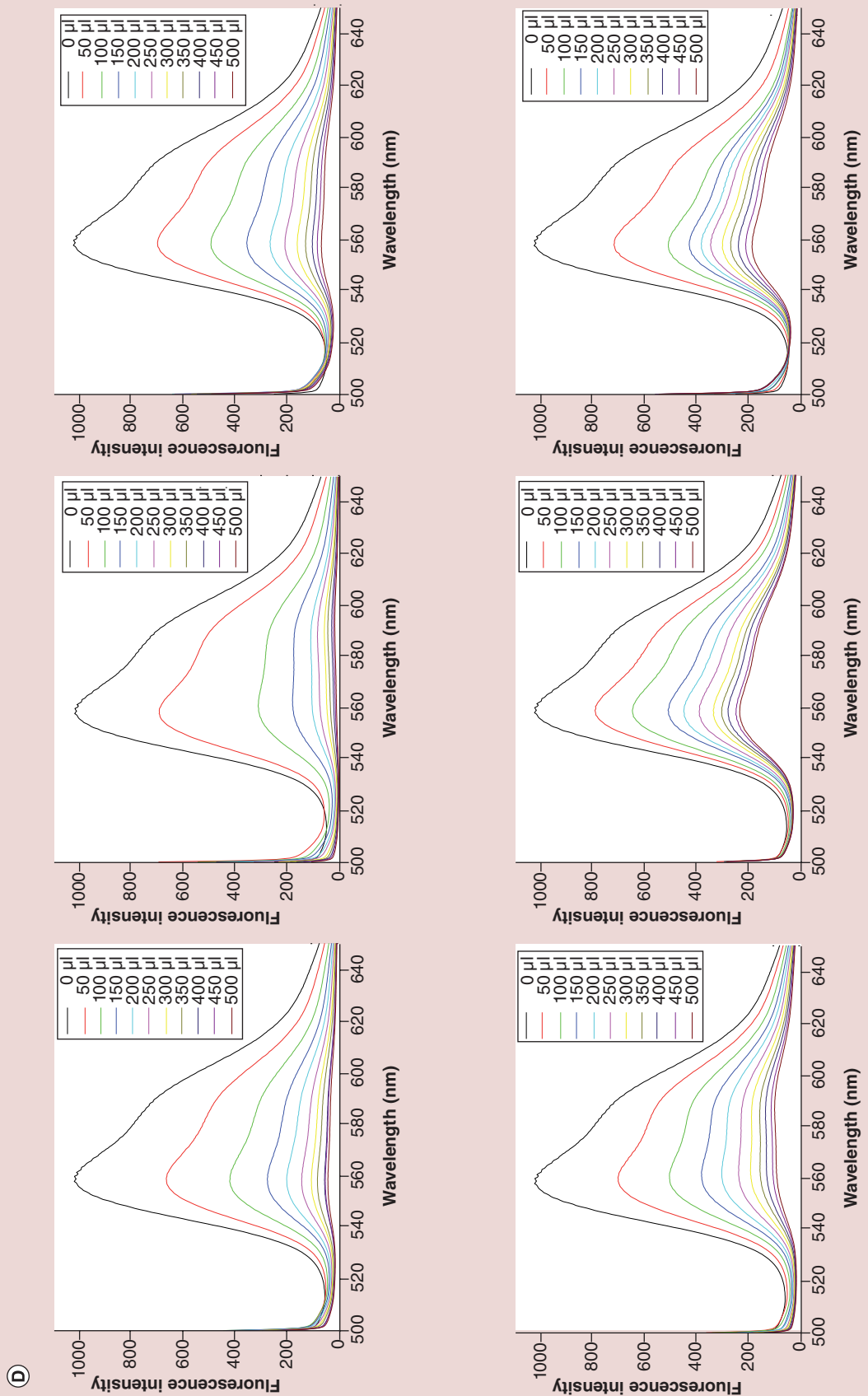


**Figure 5. Spectral fluorescence and absorption responses (for [A–C], please see above; for [D], please see facing page). (A)** Fluorescence quenching of GLT-DOX by EGCG-AuNPs. **(B)** The  $\lambda_{565}$ -to- $\lambda_{595}$  fluorescence intensity ( $I_{565}/I_{595}$ ) of GLT-DOX quenched by EGCG-AuNPs. **(C)** Overlaid emission (GLT-DOX) and absorption (EGCG-AuNPs) spectra. **(D)** Concentration-dependent fluorescence-quenching of GLT-DOX by AuNPs. AuNP: Gold nanoparticle; DOX: Doxorubicin; EGCG: Epigallocatechin gallate; GLT: Gelatin.



GLT while the stoichiometry ( $n = 1.089$ ) indicated that the protein (GLT) binds the ligand (EGCG) at 1:1 molar ratio. The equilibrium binding constants ( $K$ ) calculated from the ITC binding isotherms were  $1.13 \times 10^5 \text{ M}^{-1}$ , suggesting that the interactions between EGCG and GLT were quite strong. The negative value of entropy term ( $\Delta S$ ,  $-6.79 \text{ kJ/mol}$ ) indicates that the interaction was enthalpy driven because the molecular order increases after formation of the GLT/EGCG complex. The relatively low value of enthalpy ( $\Delta H$ ,  $-30.86 \text{ kJ/mol}$ ) implies that noncovalent interaction, in other words, hydrogen bonding, plays an essential role in the binding of EGCG with GLT to form the GLT/EGCG nanocomplex.

### Characterization of gelatin-doxorubicin conjugates

FTIR spectra of the GLT-DOX conjugates were shown in Figure 4A. Citraconic anhydride was used to react with amine groups of GLT in a ring-opening process to create more carboxyl groups. Afterward, the carboxyl groups in GLT were activated by EDC/NHS. GLT-DOX conjugates were synthesized by coupling of DOX to GLT through formation of amide bonds between the carboxyl groups of GLT and the amino groups of DOX. In the IR spectra, characteristic peaks at  $1729 \text{ cm}^{-1}$  (C=O stretch of ketone),  $1282 \text{ cm}^{-1}$  (C-C stretch) and  $1011 \text{ cm}^{-1}$  (C-O-C stretch of ether) in GLT-DOX conjugates were observed, respectively. The degree of substitution calculated from the calibration curve based on UV-Vis analysis of DOX with different concentrations was found to be 3.7 wt%.

### Characterization of layer-by-layer assembled gelatin-doxorubicin/epigallocatechin gallate-gold nanoparticles

X-ray photoelectron spectroscopy (XPS) analysis was used to investigate the formation of the EGCG-capped AuNPs and layer-by-layer assembled GLT-DOX/EGCG-AuNPs (Figure 4C). For the EGCG-AuNPs, the signal at binding energies of 88.4 and 88.0 eV were corresponding to the  $4f_{7/2}$  and  $4f_{5/2}$  orbits of  $\text{Au}^0$  (Au atoms) [30,33]. The XPS peaks of free EGCG at 286.0 (aromatic  $\text{sp}^2$ ), 290.4 eV (O-C=O) and 538.7 eV (phenolic hydroxyl) was shifted to 284.7, 289.1 and 537.0 eV after binding to the surface of the AuNPs. The results indicate the formation of GLT-DOX/EGCG-AuNPs after reacting the EGCG-AuNPs with GLT-DOX.

Figure 4B shows the zeta potential of the GLT-DOX/EGCG-AuNPs prepared by layer-by-layer assembly of GLT-DOX/EGCG multilayers on AuNPs. The zeta potential of EGCG-AuNPs is  $-20 \text{ mV}$ , indicating that the nanoparticles are surrounded by the negatively charged EGCG (polyphenol). Adsorption of the GLT-

DOX conjugate causes a change in the value of surface charge to a positive one. The sequential deposition of alternating layers of the oppositely charged GLT-DOX and EGCG onto AuNPs was observed for the change in the zeta potential of the nanoparticles with an EGCG or GLT-DOX outermost layer (Figure 4B). The result confirms the assembly of EGCG/GLT-DOX multilayers on the surface of the AuNPs.

### Characterization of nanoparticle surface energy transfer effect

Fluorescence quenching of GLT-DOX by EGCG-AuNPs was shown in Figure 5A. The fluorescence emission of GLT-DOX was significantly quenched upon the addition of EGCG<sub>0.10</sub>-Au<sub>4.0</sub> NPs due to the NSET effect [34]. In contrast, the EGCG<sub>0.10</sub>-Au<sub>4.0</sub>, EGCG<sub>0.15</sub>-Au<sub>4.0</sub> and EGCG<sub>0.10</sub>-Au<sub>2.0</sub> NPs quenched only 30–50% of GLT-DOX fluorescence intensity. Fluorescence quenching of GLT-DOX by the EGCG-AuNPs with EGCG<sub>0.10</sub>-Au<sub>4.0</sub> NPs (weaker SPR absorption) was less remarkable than those quenched by the AuNPs with stronger SPR absorption. The fluorescence quenching effect was attributed to the NSET effect caused by the formation of GLT-DOX/EGCG-AuNPs. The NSET effect was affected by the wavelength and intensity of SPR absorption of the EGCG-AuNPs. The  $\lambda_{565}$ -to- $\lambda_{595}$  fluorescence intensity ( $I_{565}/I_{595}$ ) changed when different types of EGCG-AuNPs were added to the GLT-DOX solution (Figure 5B). Figure 5C showed the overlaid emission (GLT-DOX) and absorption (EGCG-AuNPs) spectra. The EGCG<sub>0.10</sub>-Au<sub>4.0</sub> NPs having a narrow band and strong absorption at 550 nm demonstrated a more significant overlapping effect with the emission band of GLT-DOX at 565 nm than that at 595 nm. The decrease of fluorescence emissions at  $I_{565}$  and  $I_{595}$  is an evidence of the energy transfer from GLT-DOX to EGCG-AuNPs, which results in quenching of doxorubicin fluorescence. The energy transfer efficiency in fluorophore-metallic nanoparticle pairs (NSET) model is inversely proportional to the distance between the fluorophore and the nanoparticle.

In contrast to EGCG<sub>0.10</sub>-Au<sub>4.0</sub> NPs, adding EGCG<sub>0.20</sub>-Au<sub>1.0</sub> NPs or EGCG<sub>0.10</sub>-Au<sub>1.0</sub> NPs into the GLT-DOX solution did not obviously change the  $I_{565}/I_{595}$  ratio (Figure 5B). As shown in Figure 2A, a red shift and a broadening of the SPR band was observed from the absorption spectra of those EGCG-AuNPs. The emission bands of GLT-DOX at 565 and 595 nm were overlaid with the broad absorption band of EGCG-AuNPs (Figure 5C), leading to the synchronous fluorescence quenching of both emission bands (the  $I_{565}/I_{595}$  ratio is similar to that of free DOX). Concentration dependence of GLT-DOX fluorescence quenching by the EGCG<sub>0.10</sub>-Au<sub>4.0</sub> NPs was shown in Figure 5D. GLT-DOX fluorescence significantly decreased with the

increase of AuNPs concentration by adding 50–500  $\mu$ l AuNP dispersions into the GLT-DOX solution.

### Doxorubicin release & fluorescence recovery

We next investigated the effect of MMPs on fluorescence recovery and DOX release. Gelatinases A and B (MMP-2 and MMP-9) play important roles in tumor invasion, metastasis and angiogenesis through proteolysis of the extracellular matrix. MMP-2 and MMP-9 are highly expressed at the invasive edge of tumors where the nanoparticles are able to extravasate. The MMPs rich environment favors enzymatic degradation of cleavable peptide linkers and can act as a trigger mechanism for tumor-specific fluorescence ‘turn-on’ [35]. **Figure 6A** shows the recovery of quenched fluorescence of GLT-DOX due to proteolytic hydrolysis of GLT. To test whether MMP-2 can change the fluorescence properties of GLT-DOX/EGCG-AuNPs, the nanoparticles were incubated in MMP-2 containing media and the emission spectra were monitored at predetermined times. The fluorescence of DOX was not recovered by incubation of GLT-DOX/EGCG-AuNPs in MMP-2-free media. However, with the aid of proteolytic hydrolysis of GLT, MMP-2 concentration-dependent recovery of DOX fluorescence was observed after 3 h of incubation. The results indicated that the fluorescence quenching due to NSET was weakened by detachment of surface-bound GLT-DOX, consequently resulting in the fluorescence recovery.

Because MMP-2 is extremely efficient at hydrolyzing GLT, intratumoral drug release could be triggered by the gelatinases due to hydrolysis of GLT-based hydrogels or nanocarriers [36–39]. *In vitro* release studies of DOX from the GLT-DOX/EGCG-AuNPs were carried out in PBS with or without MMP-2, which simulates the conditions of physiological media and tumor site. The MMP-2 triggered DOX release from the GLT-DOX/EGCG-AuNPs due to MMP-mediated proteolysis of GLT was consistent with the recovery of fluorescence emission. **Figure 6B** shows the time-dependent MMP responsiveness of the GLT-DOX/EGCG-AuNPs in the presence of MMP-2. MMP-2 induced gradual recovery of the fluorescence from DOX at concentrations ranging from 50 to 1000 ng/ml (simulating the reported MMP-2 concentration in different tumor tissue). In presence of 50 ng/ml of MMP-2, DOX fluorescence was recovered from GLT-DOX/EGCG-AuNPs at a very slow rate. In contrast, the fluorescence intensity increased at a much faster rate with increasing the MMP-2 concentration to 1000 ng/ml due to proteolytic hydrolysis of GLT, indicating a significant release of DOX from the AuNPs. After 24 h of incubation, the release of DOX is approximately 79.4% in the medium containing 1000 ng/ml of MMP-2 as compared with 18.2%

release in those containing 50 ng/ml of MMP-2. The results suggested that the GLT-DOX/EGCG-AuNPs can be used for tumor-specific drug release triggered by MMPs such as MMP-2.

### Cellular uptake

Internalization of nanoparticles via receptor-mediated endocytosis is considered to be an effective and specific way for targeting drug delivery. The 67LR is a nonintegrin laminin receptor and is known to be overexpressed on the surface of human prostate cancer cells [21]. Cancer-overexpressed 67LR plays an important role in the metastasis of tumor cells and inducing adhesion-mediated drug resistance. The inhibitory effects of EGCG on several cancer cells are associated with the binding of EGCG to 67LR.

Human prostate cancer PC-3 cells (67LR overexpression) were used to assess targeting capabilities of GLT-DOX/EGCG-AuNPs toward the 67LR. **Figure 7A** shows a confocal microscope image of PC-3 cells treated with a FITC-labeled MLC<sub>5</sub> antibody. The green fluorescence confirmed the expression of membrane-associated 67LR on PC-3. The PC-3 cells were then exposed to GLT-DOX/EGCG-AuNPs and the internalization of the AuNPs via endocytosis was visualized using confocal laser scanning microscopy (CLSM). PC-3 cells treated with free DOX for 2 h showed the predominant accumulation of DOX in the nucleus (**Figure 7B**). The blue fluorescence in nucleus stained by DAPI was overlapped with strong red fluorescence, suggesting rapid transport of free DOX from the cytosol to the nucleus [31]. **Figure 7C** showed that GLT-DOX/EGCG-AuNPs bound to cell membranes at 1 h treatment, then accumulated in the cell cytoplasm after 2 h incubation. As shown in the supplementary imaging file (**Supplementary Figure 1**), the AuNPs were mostly accumulated in the cell cytoplasm and perinuclear area. At 4 h, DOX fluorescence was observed in nucleus because DOX has released from the AuNPs and thus was subsequently able to enter the nucleus. The apoptosis induced by GLT-DOX/EGCG-AuNPs can be observed from the decreased intensity of DAPI staining in nuclei post 4 h incubation due to significant DNA damage induced by DOX.

We next tested whether the 67LR-specific binding affinity of EGCG correlates with the internalization of the nanoparticles by PC-3 cells. Apparently, the fluorescent signal in the GLT-DOX/EGCG-AuNPs coincubated cells was stronger than that of the AuNPs coincubated and antibody treated cells after the same time of incubation (**Figure 7C**). This was most likely contributed by the targeting effect of Lam 67R-specific MLC<sub>5</sub> antibody, which could be recognized by 67LR that were overexpressed on PC-3 cells and thus mediated the cellular uptake of GLT-

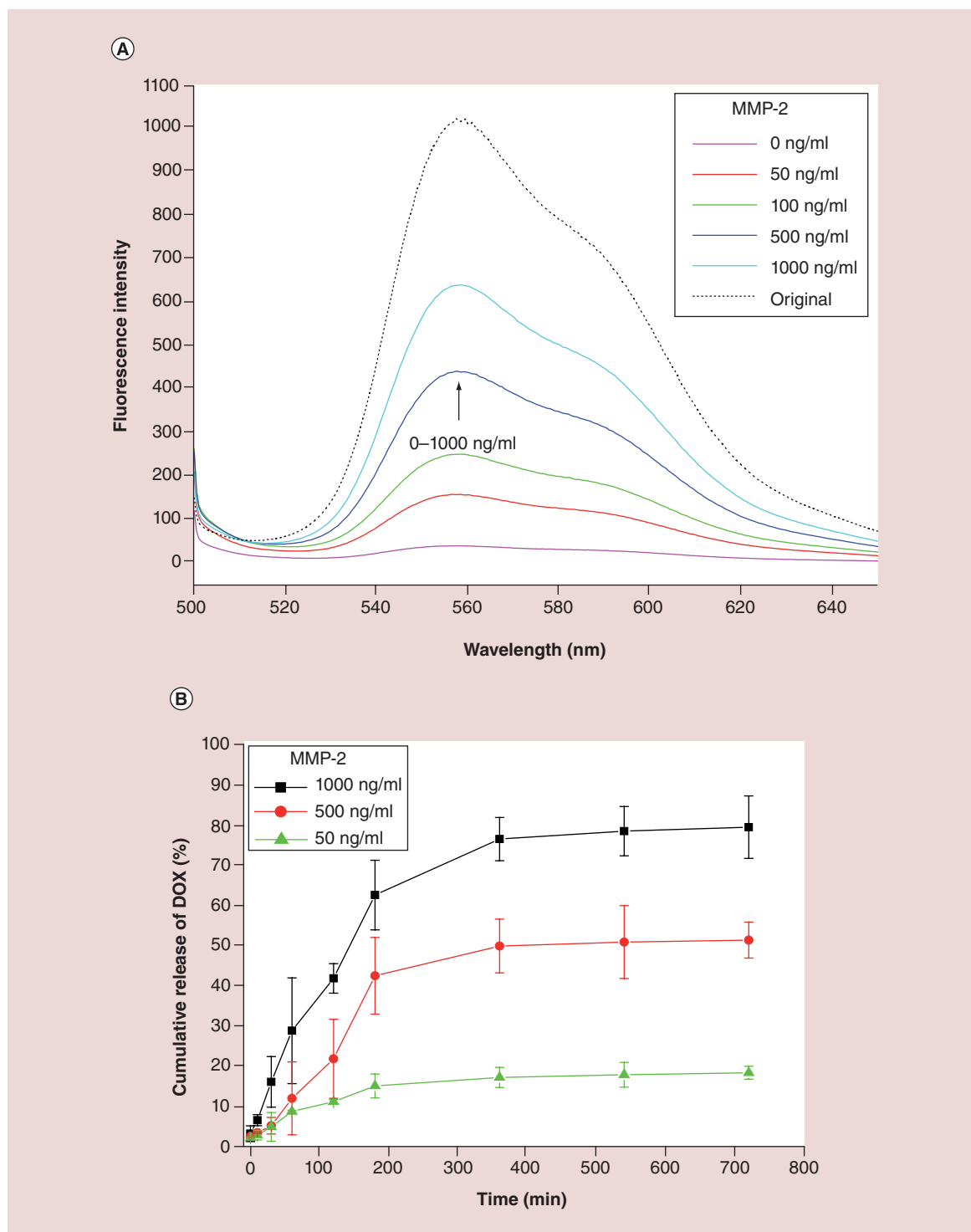


**Figure 6. Recovery of fluorescence emission.** (A) Recovery of fluorescence spectra of GLT-DOX conjugate by hydrolyzing GLT-DOX/EGCG-AuNPs in MMP-2 containing media. (B) Time dependence of fluorescence recovery in the presence of 50, 500 and 1000 ng/ml of MMP-2.

AuNP: Gold nanoparticle; DOX: Doxorubicin; EGCG: Epigallocatechin gallate; GLT: Gelatin; MMP: Matrix metalloproteinase.

DOX/EGCG-AuNPs [23,24]. As shown in Figure 7C, when co-cultured with GLT-DOX/EGCG-AuNPs, the DOX fluorescence appeared as a rim around PC-3 cells, suggest-

ing that the AuNPs bound to the cell membranes. In contrast, the red rim disappeared after treating PC-3 cells with MLC<sub>5</sub> antibody (Figure 7C). EGCG binding to the 67LR

on PC-3 cells was inhibited due to saturation of the receptors with MLuC5 antibody, leading to a reduced internalization of GLT-DOX/EGCG-AuNPs within PC-3 cells.

Moreover, TEM was used to track the intracellular distribution of the AuNPs. Cellular uptake of the AuNPs was observed after 2 h of incubation. The AuNPs were observed on cell membranes and in subcellular organelles (e.g., endosomes or lysosomes) (Figure 7D), indicating uptake of the AuNPs by acidic organelles. Some AuNPs were distributed in cytoplasm because

the AuNPs were able to escape from membrane-bound vesicles subsequent to uptake by the vesicles.

### *In vitro* antitumor activity

Chemotherapy is a traditionally used method for treating cancer; however, cell membrane is a major barrier to drug delivery. To increase the efficacy of chemotherapeutic, surface modification of AuNPs with affinity ligands can be used as potential nanocarriers for active targeting drug delivery. PC-3 human prostate cancer

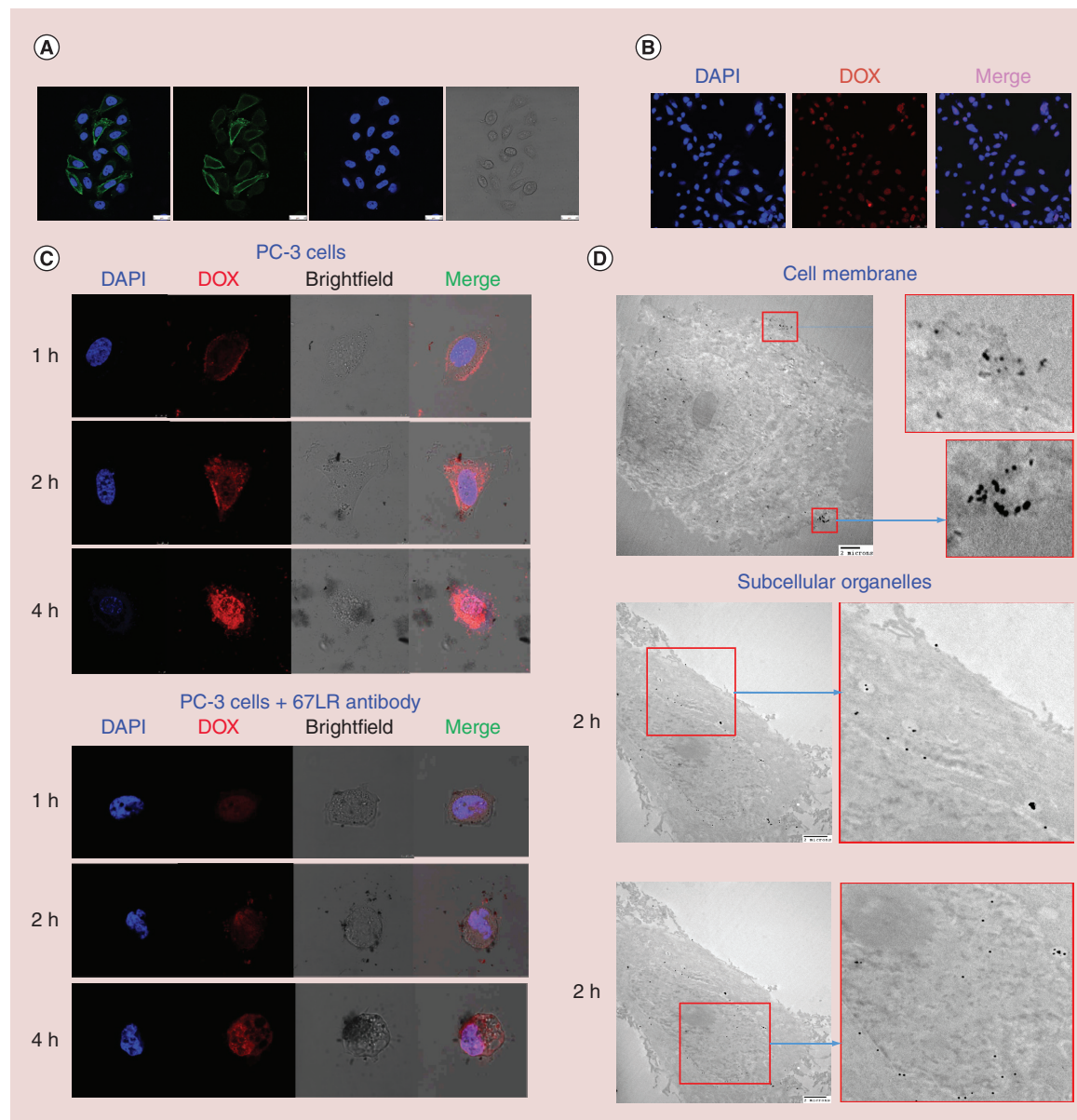


**Figure 7. Confocal microscope images.** (A) PC-3 cells stained with DAPI (blue) and treated with a FITC-labeled MLuC5 antibody (green). (B) PC-3 cells stained with DAPI (blue) and treated with free DOX (red) and (C) GLT-DOX/EGCG-AuNPs (w/ and w/o blocking 67LR receptor by antibody). (D) Transmission electron microscopy micrographs of PC-3 cells treated with GLT-DOX/EGCG-AuNPs.

67LR: 67-kDa laminin receptor; AuNP: Gold nanoparticle; DOX: Doxorubicin; EGCG: Epigallocatechin gallate; GLT: Gelatin.

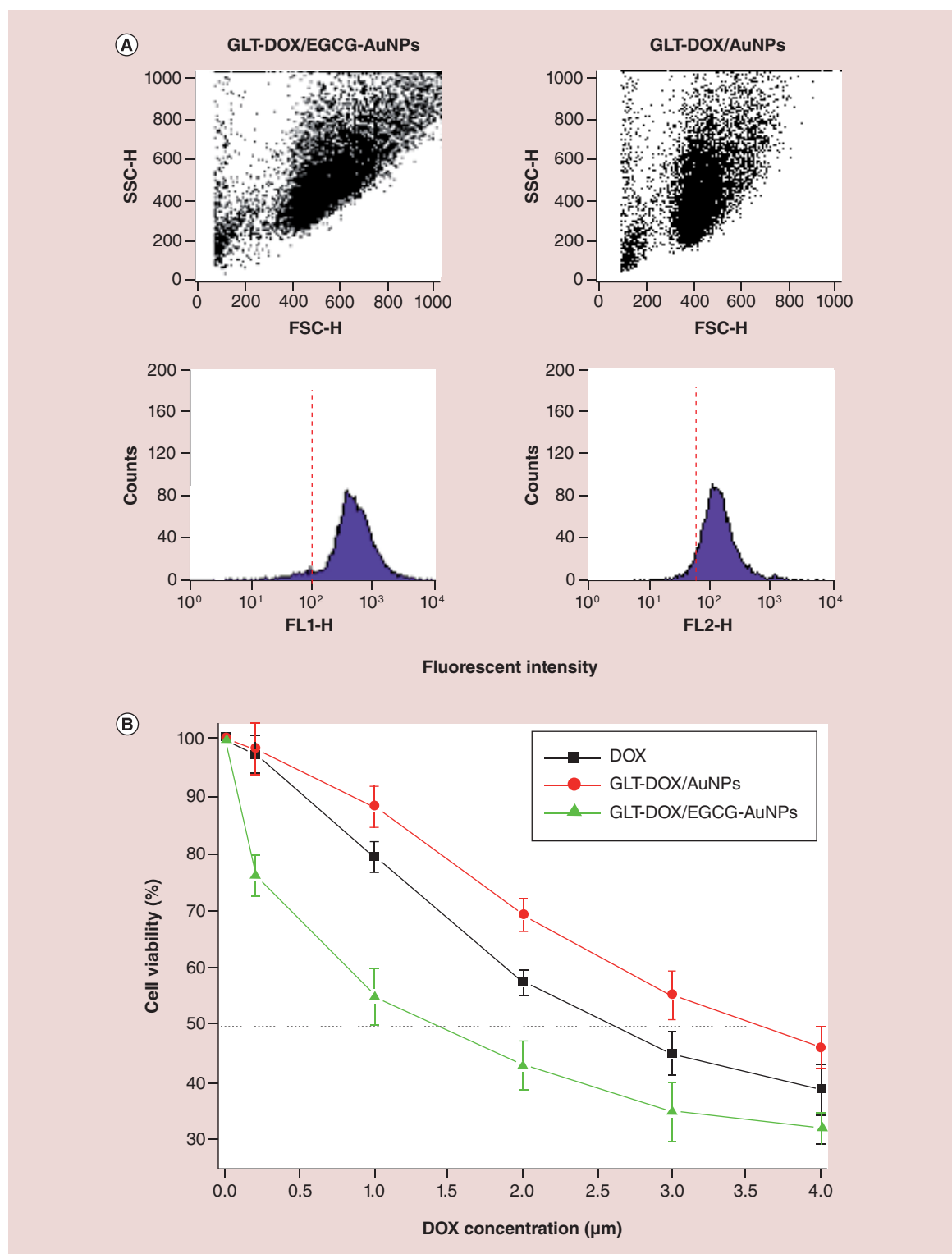
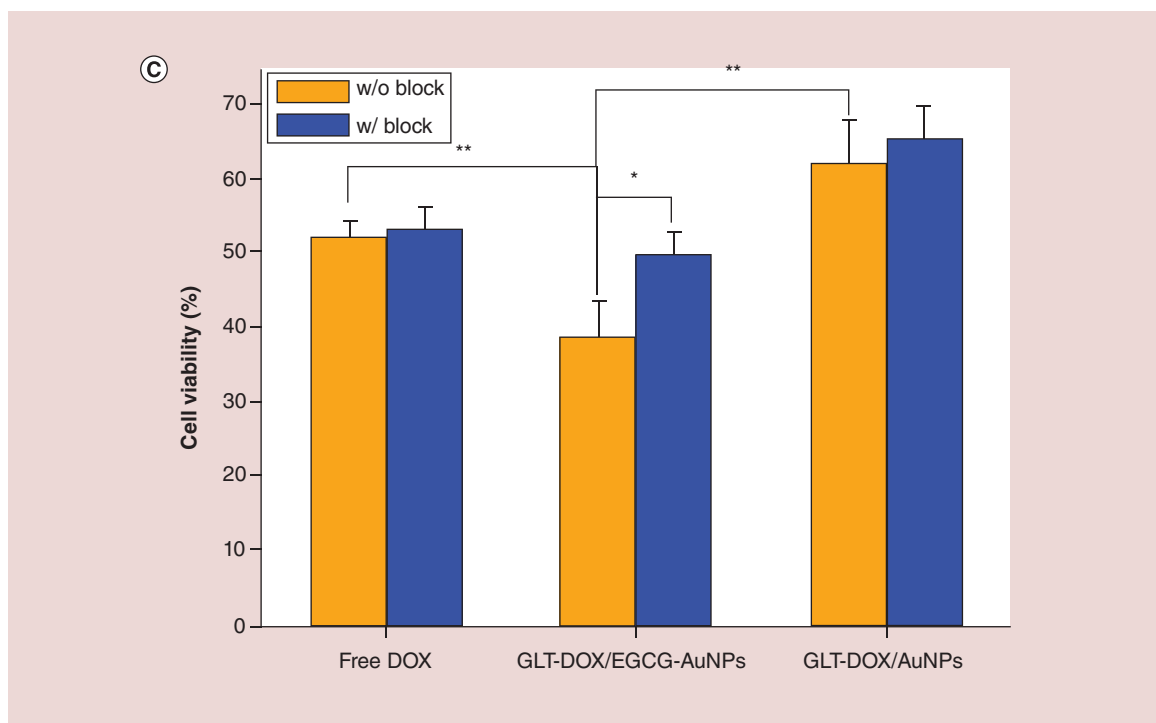


**Figure 8. Intracellular accumulation and cell viability (for [A & B], please see above; for [C], please see facing page).** (A) Flow cytometric analysis of intracellular accumulation of GLT-DOX/AuNPs and GLT-DOX/EGCG-AuNPs in PC-3 cells. (B) Cell viability of PC-3 cells treated with free DOX, GLT-DOX/AuNPs and GLT-DOX/EGCG-AuNPs at different DOX equivalents. (C) Cell viability of PC-3 cells (w/ and w/o blocked by Lam 67R-specific MLC<sub>5</sub> antibody) treated with free DOX, GLT-DOX/AuNPs and GLT-DOX/EGCG-AuNPs at 2.5  $\mu\text{M}$  DOX equivalent.

\* $p < 0.05$ .

\*\* $p < 0.01$ .

AuNP: Gold nanoparticle; DOX: Doxorubicin; EGCG: Epigallocatechin gallate; GLT: Gelatin.



cells have high metastatic potential and are overexpressed with MMP-2 and MMP-9, thus can be used for the study of MMP-responsive drug delivery [40]. In this work, EGCG were conjugated with AuNPs and the EGCG-AuNPs were further assembled with GLT-DOX to obtain the nanocomplex with small sizes. The laminin receptor targetable AuNPs are potentially beneficial in increasing DOX accumulation in PC-3 cells via receptor-mediated endocytosis. Subsequent to cellular uptake of the nanoparticles, MMP-2 and MMP-9 can hydrolyze GLT and release the drug, consequently increase the intracellular DOX level to induce apoptosis of prostate cancer PC-3 cells.

Several studies have demonstrated that EGCG can bind to the 67LR-overexpressed prostate cancer [21,24]. EGCG can also sensitize anticancer drug-induced apoptosis due to increased intracellular accumulation of some drugs [41]. As shown in Figure 8A, flow cytometric analysis revealed that an increase in the accumulation of DOX in PC-3 cells by incubation of the cells with layer-by-layer assembled GLT-DOX/EGCG-AuNPs. On the contrary, DOX delivered by GLT-DOX/AuNPs (without EGCG) was not effectively retained in PC-3 cells. Layer-by-layer modification of AuNPs with an EGCG outer surface appeared to enhance the retention of DOX by PC-3 cells. EGCG is a promising agent that can be potentially used as a targeting ligand for the development of surface-functionalized AuNPs, consequently facilitates cellular uptake of the AuNPs.

We next examine the cytotoxicity of free DOX, GLT-DOX/AuNPs and GLT-DOX/EGCG-AuNPs against

PC-3 cells using an MTT assay. Figure 8B shows the cell viability of PC-3 cells treated with free DOX and the DOX-loaded AuNPs in a dose-dependent manner. DOX is an anthracycline chemotherapeutic agent that results in cell death attributed to topoisomerase II-mediated DNA cleavage and DNA strand breaks. However, PC-3 cells are highly resistant to DOX [42]. Free DOX exhibited moderate cytotoxicity against the PC-3 cells with an  $IC_{50}$  value of 2.6  $\mu$ M (Figure 8B). GLT-DOX/AuNPs showed a higher  $IC_{50}$  value (3.6  $\mu$ M DOX equivalent) compared with that of free DOX because DOX must diffuse from the cytoplasm to the nucleus when incorporated to the AuNPs.

It is worth noting that a more significant cytotoxic effect was observed for PC-3 cells incubated with the GLT-DOX/EGCG-AuNPs compared with GLT-DOX/AuNPs ( $p < 0.01$ ). GLT-DOX/EGCG-AuNPs showed a lower  $IC_{50}$  value (1.4  $\mu$ M DOX equivalent) compared with that of free DOX and GLT-DOX/AuNPs. GLT-DOX/EGCG-AuNPs can increasingly accumulate DOX in PC-3 cells, thus the NPs are more effective than free DOX and GLT-DOX/AuNPs in inhibiting the cell proliferation. The receptor-mediated cellular uptake of NPs is exerted by binding of EGCG to 67LR, a high-affinity nonintegrin laminin receptor overexpressed in PC-3 cells. Several studies reported that EGCG can reduce PC-3 cell viability due to the inhibitory effect of EGCG on tumor cells proliferation. EGCG inhibits PC-3 prostate cancer cell proliferation via MEK-independent ERK1/2 activation [43]. Moreover, EGCG induced the activation

of initiator caspase-8, leading to proteolytic cleavage of PARP [44]. EGCG-loaded chitosan NPs have been reported to enhance antiproliferative and proapoptotic effects on human prostate cancer cells [45]. Additionally, combination of DOX and EGCG showed a synergistic inhibitory effect on the growth of human prostate cell lines [41]. Combination of DOX and EGCG in the layer-by-layer assembled AuNPs may enhance the inhibition of PC3 cell proliferation due to receptor-mediated targeting and synergistic effects.

EGCG–membrane interaction may influence the fluidity of cellular membranes, leading to the enhanced internalization of nanoparticles [46]. Thus, the enhanced anticancer efficiency of DOX by GLT-DOX/EGCG-AuNPs can be attributed to the effects of receptor-binding and EGCG–membrane interaction. We further determined if the growth inhibitory effects of GLT-DOX/EGCG-AuNPs affected by blocking 67LR. Treating PC-3 cells with Lam 67R-specific MLC<sub>5</sub> antibody, we observed increased cell viability of the cells treated with GLT-DOX/EGCG-AuNPs (2.5 μM DOX equivalent) after 24 h of incubation ( $p < 0.05$ ). The results suggest that the receptor recognition combined with MMP-2-mediated drug release has considerable potential for effectively delivering the NPs into PC-3 cells to achieve concentrated local DOX release, consequently resulting in improved anticancer activity in the cancer cell.

## Conclusion

In this study, EGCG was used to chelate with Au<sup>3+</sup> ions and subsequently reduced the chelated Au<sup>3+</sup> ions to Au<sup>0</sup> atoms, leading to formation of EGCG-capped gold nanoparticles (EGCG-AuNPs). EGCG-AuNPs can be used to bind GLT-DOX, producing GLT-DOX/EGCG-AuNPs exhibiting MMP-responsive property and PC-3-targeting ability. Such aN AuNP-based drug delivery system can significantly inhibit the growth of PC-3 cells, owing to the laminin receptor-mediated endocytosis and the MMP-responsive release of DOX. The GLT-DOX/EGCG-AuNPs served multiple functions by probing the intracellular DOX release and inhibiting PC-3 cells proliferation.

## Future perspective

Nanotechnology has been used as an efficient approach for the development of a safe and efficient delivery system in cancer therapy. Layer-by-layer assembly is a possible method to prepare functionalized nanoparticles for imaging, targeting, drug delivery and drug release not formerly feasible. AuNPs have long been regarded as low toxic nanocarriers and nonviral vectors for drug and gene delivery. AuNPs are already being examined in clinical trials for applications in biomedical imaging, and photothermal and photodynamic therapy. Surface

modification of AuNPs can diminish immunogenic responses, increase their circulation half-lives, improve specific targeting and reduce dosing requirements. DOX has severe systemic toxicity and other undesirable side effects such as cardiotoxicity and myelosuppression, which is considered to have a narrow therapeutic index. In respect to clinical use of DOX in treating prostate cancer, the major challenge will be due to the fact that DOX can be poorly delivered locally to the site of prostate cancer. Medical scientists have encountered problems with fast clearance from the circulation and poor tumor uptake of the drug that need to be overcome. It may be expected that therapeutic uses of functionalized AuNPs will be achieved in the coming years. To provide the AuNPs with tumor-specific targeting capability, we prepre EGCG-functionalized AuNPs. EGCG is a ligand of a high affinity nonintegrin laminin receptor (67LR) overexpressed in PC-3 prostate cancer cells. This design might find potential applications in improving the therapeutic potential for prostate cancer by the receptor-mediated tumor targeting and the synergistic effect of the combination of EGCG and DOX chemotherapy. However, preliminary tests in animal models and clinical translation of the newly developed nanomedicine should be evaluated to validate its therapeutic potential.

## Supplementary data

To view the supplementary data that accompany this paper, please visit the journal website at: [www.futuremedicine.com/doi/full/10.2217/NNM.15.183](http://www.futuremedicine.com/doi/full/10.2217/NNM.15.183)

## Acknowledgements

The authors thank AC Chun, CM Lee and HM Chen (Core Facility Center, Taipei Medical University) for technical support in CLSM 3-D imaging and TEM analysis.

## Financial & competing interests disclosure

This work was supported by a grant (NTUT-TMU-103-13) from Taipei Medical University and National Taipei University of Technology, Taiwan. The authors have no other relevant affiliations or financial involvement with any organization or entity with a financial interest in or financial conflict with the subject matter or materials discussed in the manuscript apart from those disclosed.

No writing assistance was utilized in the production of this manuscript.

## Ethical conduct of research

The authors state that they have obtained appropriate institutional review board approval or have followed the principles outlined in the Declaration of Helsinki for all human or animal experimental investigations. In addition, for investigations involving human subjects, informed consent has been obtained from the participants involved.

## Executive summary

**Background**

- There are some disadvantages caused by cancer treatment with clinically used anticancer drugs. Active targeting can be achieved by conjugating nanocarriers with ligands that bind to overexpressed antigens or receptors on the surface of cancer cells.

**Aim**

- Preparation of gold nanoparticles (AuNPs) coated with epigallocatechin gallate (EGCG) and gelatin-doxorubicin conjugate (GLT-DOX).
- Enhancement of intracellular delivery of the DOX-loaded AuNPs by Lam 67R receptor-mediated endocytosis.
- Development of functional AuNPs for fluorescence imaging and inhibition of prostate cancer cell growth.

**Results**

- AuNPs alternatively coated with EGCG and DOX-GLT conjugates were successfully prepared by a layer-by-layer assembly method.
- DOX-GLT/EGCG AuNPs effectively quenched the fluorescence of DOX due to the nanoparticle surface energy transfer effect.
- *In vitro* release of DOX from DOX-GLT/EGCG AuNPs was triggered by MMP-2 because GLT was easily degraded by the enzyme.
- The enzyme-responsive intracellular release of DOX could be tracked in real time by monitoring the recovery of the fluorescence signal of DOX.
- The AuNPs significantly inhibit the cancer cell proliferation because they were increasingly uptaken by the cells via Lam 67R receptor-mediated endocytosis.

**Conclusion**

- Our results confirmed that Lam 67R receptor-mediated delivery of DOX using the DOX-GLT/EGCG AuNPs enhanced cellular uptake of DOX. MMP-2 triggered DOX release from the AuNPs and the apoptosis of human prostate cells was improved by a synergistic inhibitory effect of EGCG. The DOX-GLT/EGCG AuNPs may have clinical application in the treatment of prostate cancer cells.

**References**

- 1 Cai LQ, Xu GF, Shi CY, Guo DD, Wang X, Luo JT. Telodendrimer nanocarrier for co-delivery of paclitaxel and cisplatin: a synergistic combination nanotherapy for ovarian cancer treatment. *Biomaterials* 37, 456–468 (2015).
- 2 Wang LM, Lin XY, Wang J *et al.* Novel insights into combating cancer chemotherapy resistance using a plasmonic nanocarrier: enhancing drug sensitiveness and accumulation simultaneously with localized mild photothermal stimulus of femtosecond pulsed laser. *Adv. Funct. Mater.* 24, 4229–4239 (2014).
- 3 Nguyen T, Tekrony A, Yaehne K, Cramb DT. Designing a better theranostic nanocarrier for cancer applications. *Nanomedicine* 9, 2371–2386 (2014).
- 4 Chen X, Soeriyadi AH, Lu X *et al.* Dual bioresponsive mesoporous silica nanocarrier as an “and” logic gate for targeted drug delivery cancer cells. *Adv. Funct. Mater.* 24, 6999–7006 (2014).
- 5 Van de Broek B, Devoogdt N, D’Hollander A *et al.* Neuropilin-1-targeted gold nanoparticles enhance therapeutic efficacy of platinum(IV) drug for prostate cancer treatment. *ACS Nano* 8, 4205–4220 (2014).
- 6 De Jong WH, Hagens WI, Krystek P *et al.* Particle size-dependent organ distribution of gold nanoparticles after intravenous administration. *Biomaterials* 29, 1912–1919 (2008).
- 7 Marchesano V, Hernandez Y, Salvenmoser W *et al.* Imaging inward and outward trafficking of gold nanoparticles in whole animals. *ACS Nano* 7, 2431–2442 (2013).
- 8 Nicol JR, Dixon D, Coulter JA. Gold nanoparticle surface functionalization: a necessary requirement in the development of novel nanotherapeutics. *Nanomedicine* 10, 1315–1326 (2015).
- 9 Li WW, Chen XY. Gold nanoparticles for photoacoustic imaging. *Nanomedicine* 10, 299–320 (2015).
- 10 Chen WH, Xu XD, Jia HZ *et al.* Therapeutic nanomedicine based on dual-intelligent functionalized gold nanoparticles for cancer imaging and therapy *in vivo*. *Biomaterials* 34, 8798–8807 (2013).
- 11 Barenholz Y. Doxil<sup>®</sup> – the first FDA-approved nano-drug: lessons learned. *J. Control. Release* 160, 117–134 (2012).
- 12 Tang S, Yin Q, Zhang ZW *et al.* Co-delivery of doxorubicin and RNA using pH-sensitive poly (beta-amino ester) nanoparticles for reversal of multidrug resistance of breast cancer. *Biomaterials* 35, 6047–6059 (2014).
- 13 Batrakova EV. Overcoming multidrug resistance using silica nanoparticles PEG-b-PLA polymeric micelles loaded with doxorubicin. *Nanomedicine* 6, 1492–1493 (2011).
- 14 Wang F, Wang YC, Dou S *et al.* Doxorubicin-tethered responsive gold nanoparticles facilitate intracellular drug delivery for overcoming multidrug resistance in cancer cells. *ACS Nano* 5, 3679–3692 (2011).
- 15 Meng H, Xue M, Xia T *et al.* Use of size and a copolymer design feature to improve the biodistribution and the enhanced permeability and retention effect of doxorubicin-loaded mesoporous silica nanoparticles in a murine xenograft tumor model. *ACS Nano* 5, 4131–4144 (2011).
- 16 Yang E, Qian WP, Cao ZH *et al.* Theranostic nanoparticles carrying doxorubicin attenuate targeting ligand

- specific antibody responses following systemic delivery. *Theranostics* 5, 43–61 (2015).
- 17 Yu PC, Yu HJ, Guo CY *et al.* Reversal of doxorubicin resistance in breast cancer by mitochondria-targeted pH-responsive micelles. *Acta Biomater.* 14, 115–124 (2015).
  - 18 Khan N, Bharali DJ, Adhami VM *et al.* Oral administration of naturally occurring chitosan-based nanoformulated green tea polyphenol EGCG effectively inhibits prostate cancer cell growth in a xenograft model. *Carcinogenesis* 35, 415–423 (2014).
  - 19 Rocha S, Generalov R, Pereira MD *et al.* Epigallocatechin gallate-loaded polysaccharide nanoparticles for prostate cancer chemoprevention. *Nanomedicine* 6, 79–87 (2011).
  - 20 Harper CE, Patel BB, Wang J, Eltoum IA, Lamartiniere CA. Epigallocatechin-3-gallate suppresses early stage, but not late stage prostate cancer in TRAMP mice: mechanisms of action. *Prostate* 67, 1576–1589 (2007).
  - 21 Shukla R, Chanda N, Zambre A *et al.* Laminin receptor specific therapeutic gold nanoparticles (198AuNP-EGCG) show efficacy in treating prostate cancer. *Proc. Natl Acad. Sci. USA* 109, 12426–12431 (2012).
  - 22 Hsieh DS, Wang H, Tan SW *et al.* The treatment of bladder cancer in a mouse model by epigallocatechin-3-gallate-gold nanoparticles. *Biomaterials* 32, 7633–7640 (2011).
  - 23 Kumazoe M, Sugihara K, Tsukamoto S *et al.* 67-kDa laminin receptor increases cGMP to induce cancer-selective apoptosis. *J. Clin. Invest.* 123, 787–799 (2013).
  - 24 Fujimura Y, Sumida M, Sugihara K *et al.* Green tea polyphenol EGCG sensing motif on the 67-kDa laminin receptor. *PLoS ONE* 7, e37942 (2012).
  - 25 Chung JE, Tan S, Gao SJ *et al.* Self-assembled micellar nanocomplexes comprising green tea catechin derivatives and protein drugs for cancer therapy. *Nat. Nanotechnol.* 9, 907–912 (2014).
  - 26 Wong C, Stylianopoulos T, Cui JA *et al.* Multistage nanoparticle delivery system for deep penetration into tumor tissue. *Proc. Natl Acad. Sci. USA* 108, 2426–2431 (2011).
  - 27 Xu JH, Gao FP, Liu XF *et al.* Supramolecular gelatin nanoparticles as matrix metalloproteinase responsive cancer cell imaging probes. *Chem. Commun.* 49, 4462–4464 (2013).
  - 28 Shutava TG, Balkundi SS, Vangala P *et al.* Layer-by-layer-coated gelatin nanoparticles as a vehicle for delivery of natural polyphenols. *ACS Nano* 3, 1877–1885 (2009).
  - 29 Neupane MP, Lee SJ, Park IS *et al.* Synthesis of gelatin-capped gold nanoparticles with variable gelatin concentration. *J. Nanopart. Res.* 13, 491–498 (2011).
  - 30 Zhu H, Du ML, Zou ML *et al.* Facile and green synthesis of well-dispersed Au nanoparticles in PAN nanofibers by tea polyphenols. *J. Mater. Chem.* 22, 9301–9307 (2012).
  - 31 Wu H, Huang X, Gao MM, Liao XP, Shi B. Polyphenol-grafted collagen fiber as reductant and stabilizer for one-step synthesis of size-controlled gold nanoparticles and their catalytic application to 4-nitrophenol reduction. *Green Chem.* 13, 651–658 (2011).
  - 32 Usha R, Ramasami T. Structure and conformation of intramolecularly cross-linked collagen. *Colloids Surf B Biointerfaces* 41, 21–24 (2005).
  - 33 Jin WP, Xu W, Ge HH, Li Y, Li B. Polyphenol-gelatin nanoparticles as reductant and stabilizer for one-step synthesis of gold nanoparticles and their interfacial behavior. *RSC Adv.* 5, 26496–26503 (2015).
  - 34 Hong Y, Ku M, Heo D *et al.* Molecular recognition of proteolytic activity in metastatic cancer cells using fluorogenic gold nanoprobe. *Biosens. Bioelectron.* 57, 171–178 (2014).
  - 35 Barazzouk S, Kamat PV, Hotchandani S. Photoinduced electron transfer between chlorophyll a and gold nanoparticles. *J. Phys. Chem. B* 109, 716–723 (2005).
  - 36 Chen WH, Luo GF, Lei Q *et al.* MMP-2 responsive polymeric micelles for cancer-targeted intracellular drug delivery. *Chem. Commun.* 51, 465–468 (2015).
  - 37 Chen WH, Xu XD, Jia HZ *et al.* Therapeutic nanomedicine based on dual-intelligent functionalized gold nanoparticles for cancer imaging and therapy *in vivo*. *Biomaterials* 34, 8798–8807 (2013).
  - 38 van Rijt SH, Bolukbas DA, Argyo C *et al.* Protease-mediated release of chemotherapeutics from mesoporous silica nanoparticles to *ex vivo* human and mouse lung tumors. *ACS Nano* 9, 2377–2389 (2015).
  - 39 Dorresteyn R, Billecke N, Schwendy M *et al.* Polylactide-block-polypeptide-block-poly lactide copolymer nanoparticles with tunable cleavage and controlled drug release. *Adv. Funct. Mater.* 24, 4026–4033 (2014).
  - 40 Trudel D, Fradet Y, Meyer F, Harel F, Tetu B. Significance of MMP-2 expression in prostate cancer: an immunohistochemical study. *Cancer Res.* 63, 8511–8515 (2003).
  - 41 Stearns ME, Amatangelo MD, Varma D, Sell C, Goodyear SM. Combination therapy with epigallocatechin-3-gallate and doxorubicin in human prostate tumor modeling studies inhibition of metastatic tumor growth in severe combined immunodeficiency mice. *Am. J. Pathol.* 177, 3169–3179 (2010).
  - 42 Kelly MM, Hoel BD, Voelkel-Johnson C. Doxorubicin pretreatment sensitizes prostate cancer cell lines to TRAIL induced apoptosis which correlates with the loss of c-FLIP expression. *Cancer Biol. Ther.* 5, 520–527 (2002).
  - 43 Albrecht DS, Clubbs EA, Ferruzzi M, Bomser JA. Epigallocatechin-3-gallate (EGCG) inhibits PC-3 prostate cancer cell proliferation via MEK-independent ERK1/2 activation. *Chem. Biol. Interact.* 171, 89–95 (2008).
  - 44 Gupta S, Hastak K, Afaq F, Ahmad N, Mukhtar H. Essential role of caspases in epigallocatechin-3-gallate-mediated inhibition of nuclear factor kappa B and induction of apoptosis. *Oncogene* 23, 2507–2522 (2004).
  - 45 Shabana SM, Siddiqui IA, Khan N *et al.* Excellent anti-proliferative and pro-apoptotic effects of (-)-epigallocatechin-3-gallate encapsulated in chitosan nanoparticles on human prostate carcinoma cells. *J. Pharmaceut. Pharmacol.* 2, 1–8 (2014).
  - 46 Lu YC, Luo PC, Huang CW *et al.* Augmented cellular uptake of nanoparticles using tea catechins: effect of surface modification on nanoparticle-cell interaction. *Nanoscale* 6, 10297–10306 (2014).